Author's Response to the Editor and Referees' Reports

Dec. 3, 2018

Manuscript: **An Energy Balance Model for Paleoclimate Transitions**

The authors thank the two reviewers for their constructive criticisms and for pointing out much useful recent work on paleoclimates. We strongly believe the reviewers' suggestions have contributed substantially to improving the manuscript.

We have made major modifications to the manuscript based on the reviewers' suggestions and questions. We have previously responded to each of the reviewers' reports, and those responses have been published on-line with the journal. Those responses dealt with the reviewers' issues in a point-by-point manner; we will not repeat those responses here. However, we have made the changes to the manuscript as outlined in those responses. Here we describe the major changes to the manuscript. To begin, we respond to the two major points made by Reviewer 2:

I believe there is room for large improvement in two major directions:

1. *In demonstrating the validation of the EBM for present day and for simple sensitivity experiments as doubling CO2 and glacial/interglacial transition to test the sensitivity of EBM before going to deeper time climate transitions.*

2. *Depicting a better and updated insight in the recent bibliography concerning each paradox to show more clearly what is the added value of these new simulations in understanding major transitions.*

With regard to the first point, we have calibrated the EBM with modern published data and have given this calibration in Appendix A. In addition, we have calculated the Equilibrium Climate Sensitivity (ECS) (the equilibrium surface temperature change due to a doubling in CO_2 levels) for our EBM in Appendix B. The calculated value is $3.3^\circ\mathrm{C}$, which is in excellent agreement with accepted values published by the IPCC. (In our original response to the reviewers we had indicated we would publish an ECS calculation in a subsequent paper, but since the editor requested specifically that we meet this suggestion of the referee, we have done so in this manuscript. We now agree that it strengthens the validity of EBM.) With regard to the second point, we have expanded the bibliography (about doubling the number of citations), which now includes the many papers pointed out by both reviewers as well as other relevant papers we have found since. We have improved the discussion in the Introduction and throughout the paper by referring to the results of these additional works.

We believe that the primary contribution of our manuscript is showing that a relatively simple model of the climate that incorporates water vapor feedback, ice albedo feedback, and the contribution of carbon dioxide as a greenhouse gas, has multiple equilibrium states, both warm and frozen, and that rapid transitions (bifurcations) between these states occur due to relatively small changes in the forcing parameters. We suggest that the sudden changes in climate in the past at both poles is a manifestation of this mathematical reality of bifurcations of equilibria. We have tried to highlight this as the primary contribution of this work.

Detailed Description of Manuscript Changes

We have provided below the output of "latexdiff", a tool that compares LaTeX source files. The pdf output shows explicitly the alterations made between the original version and the version we are re-submitting at this time. Below we describe these changes. Besides the major changes mentioned below, we made many minor alterations in wording and phrasing in order to improve clarity and flow. We will not comment further on those changes.

1. The introduction (Section 1) was substantially complemented with references to other research work. In addition, we have highlighted more clearly the results of this paper. At the end of this section we mention the two new appendices where the model is calibrated and where the ECS value is computed.

2. Section 2 has been thoroughly re-written. We have moved the determination of numerical values of parameters to Appendix A, so that Section 2 is shorter and focuses on the mathematical model itself. This addresses the one suggestion of the first reviewer to shorten the technical section.

3. We have altered the EBM model slightly in order to allow for calibration with modern data. In particular, the model now accounts for reflection of sunlight from the atmosphere back into space, and the direct absorption of sunlight by the

atmosphere. This has led to the introduction of two new parameters ξ_R and ξ_A, which represent the fraction of incoming solar radiation that is reflected and absorbed, respectively.

4. We have updated Figure 1–3 of Section 2 (old Figures 1,3, and 4) to reflect the modified model.

5. We have changed the definition of the symbol F_S to now be the solar radiation striking the surface, rather than that absorbed by the surface.

6. We have changed how we model the conduction/convection/evapotranspiration of heat from the surface to the atmosphere, F_C. The previous manuscript simply had F_C as a constant that we altered depending on the region of the earth to which the model was being applied. However, F_C is certainly dependent on surface temperature, and since we are considering applications where surface temperature changes from below to above freezing it makes sense to model this explicitly. We also found that to calibrate the model to modern data, it was necessary to model F_C as temperature dependent. The precise way we have modelled this dependence is given in Section 2.1, and the parameter values for this functional form are calibrated in Appendix A to modern data.

7. Table 1 has been updated with the new model parameters. A few of the former entries in the table, that were only used as intermediate values, have been removed in order to keep the table to one page. All values for the model parameters are still present in the Table.

8. In order to calibrate the model to modern data, we have also added absorption of infrared radiation due to liquid and solid water in clouds. The previous model ignored this contribution. However, cloud absorption constitutes about 25% of total absorption and so to calibrate the model with published energy balance values, it was necessary to include this contribution. Since there is virtually no information on paleoclimate cloud cover, we have kept this value as a constant even though it clearly will depend on surface temperature, surface topography, and latitude. We did try modelling the dependence of cloud absorption on surface temperature, like for F_C, but found no qualitative change in our results and so have left cloud absorption as a global and temporal constant contribution.

9. Section 3.1 and Section 3.2 have been swapped in the new manuscript so that the Pliocene Paradox is treated first.

10. Figures 4–8 in Section 3 (old Figures 5–9) have been re-drawn to correspond to the modified model. The values of the atmospheric and ocean heat transport forcings, F_A and F_O, are modified slightly from the previous model in order to compensate for the model changes introduced. The qualitative features of these figures have not changed. In particular, the bifurcations remain present, where warm equilibria disappear in a saddle-node.

11. Section 4, the conclusion, has had a few minor alterations.

12. Appendices A and B are new. Appendix A gives the empirical calibration of the EBM model to published modern data. Some of this material is new, corresponding to new aspects of the modified model like atmospheric reflection and absorption of sunlight, and some of the material has been moved here from the old Section 2, so that all numerical calibration is in one place.

13. Figure A1 was Figure 2b in the old version. Figure A2 is a new figure depicting the dependence of F_C on temperature.

14. Appendix B gives the equilibrium climate sensitivity (ECS) calculation for the EBM. It predicts an ECS value of $3.3^\circ\mathrm{C}$ for a doubling of CO_2 concentration from 270 ppm to 540 ppm. Figure B1 is new, depicting the ECS.

15. The bibliography has increased from 53 to 107 entries.

Again, we thank the reviewers for their very thoughtful and detailed reviews. We believe that the revised manuscript addresses all of the issues raised by them and the editor. We respectfully re-submit the manuscript for publication.

Sincerely,

Brady Dormans, William F. Langford, and Allan R. Willms

An Energy Balance Model for Paleoclimate Transitions

Brady Dortmans, William F. Langford, and Allan R. Willms

Department of Mathematics and Statistics, University of Guelph, 50 Stone Road West, Guelph, ON, Canada N1G 2W1

Correspondence to: W. F. Langford (wlangfor@uoguelph.ca)

Abstract. A new energy balance model (EBM) is presented and is used to study Paleoclimate transitions. While most previous EBMs dealt only with the globally averaged climate, this new EBM has three variants: Arctic, Antarctic and Tropical climates. ~~This~~ The EBM incorporates the greenhouse warming effects of both carbon dioxide and water vapour, and also includes ice-albedo feedback and evapotranspiration. The main conclusion to be ~~drawn from the~~ inferred from this EBM is that the climate system ~~possesses~~ may possess multiple equilibrium states, both warm and frozen, which coexist mathematically. While the actual climate can exist in only one of these states at any given time, the EBM suggests that climate can undergo transitions between the states, via mathematical saddlenode bifurcations. This paper proposes that such bifurcations have actually occurred in Paleoclimate transitions. The EBM is applied to the study of the *Pliocene Paradox*, the *Glaciation of Antarctica* and the so-called *warm, equable climate problem* of both the mid-Cretaceous Period and the Eocene Epoch. In all cases, the EBM is in qualitative agreement with the geological record.

1 Introduction

For ~~most~~ approximately 75% of the last 540 million years of the paleoclimate history of the Earth, the climate of both polar regions was mild and free of permanent ice-caps; Cronin (2010); Crowley (2000); Huber et al. (2000). Today, both North and South Poles are ice-capped; however, there is overwhelming evidence that these polar ice-caps are ~~now~~ melting. The Arctic is warming faster than any other region on Earth. The formation of the present-day Arctic and Antarctic ice-caps occurred abruptly, at widely separated times in the geological history of the Earth. This paper explores some of the the underlying mechanisms and forcing factors that have caused climate transitions in the past. The ~~knowledge~~ understanding gained here will be applied in a subsequent paper to the important problem of forecasting anthropogenic climate change.

We present a new two-layer energy balance model (EBM) for the climate of the Earth. ~~The understanding~~ General knowledge of climate and of climate change has been advanced by many studies employing ~~EBMs: (Budyko (1968); Dortmans et al. (2017); Kaper and~~ simple EBMs (Budyko (1968); Kaper and Engler (2013); McGeehee and Lehman (2012); North et al. (1981); Payne et al. (2015); Sagan a). In general, these ~~simple~~ EBMs facilitate exploration of the relationship between specific climate forcing mechanisms and the resulting climate changes. The EBM presented here includes a more accurate representation of the role of greenhouse gases

in climate change than has been the case for previous ~~EBM's~~EBMs. The model is based on fundamental principles of atmospheric physics, such as the Beer-Lambert Law, the Stefan-Boltzmann Law, the Clausius-Clapeyron equation and the ideal gas equation. In particular, the modelling of water vapour acting as a greenhouse gas in the atmosphere, presented in Subsection 2.3.3, is more physically accurate that in previous EBMs and it ~~leads to new insights for climate change~~shows that *water vapour feedback* is important in climate change. Also, *ice-albedo feedback* plays a central role in this EBM. The nonlinearity of this EBM leads to *bistability* (existence of multiple stable equilibrium states), to *hysteresis* (the climate state realized in the model depends on the past history) and to *bifurcations* (abrupt transitions from one state to another). Previous climate models exhibiting multiple equilibrium states have been studied for example by North et al. (1981); Paillard (1998); Ferreira et al. (2011); Thorndik . Forcing factors that are included explicitly in the model include insolation, CO_2 concentration, relative humidity, evapotranspiration, ocean heat transport and atmospheric heat transport. Other factors that may affect climate change, such as geography, precipitation, vegetation, and continental drift are not included explicitly in the EBM, but are present only implicitly in so far as they affect those included factors.

During the ~~early~~ Pliocene Epoch, ~~3–5~~ 2.6–5.3 Ma, the climate of the Arctic region of Earth changed abruptly from ice-free to ice-capped. The major climate forcing factors ~~then~~ (solar constant, orbital parameters, CO_2 concentration and locations of the continents) were all very similar to today; Fedorov et al. (2006, 2010); Haywood et al. (2009); Lawrence et al. (2009); De Schepper et al. (. Therefore, it is difficult to explain why the early Pliocene climate was so different from that of today. That problem ~~is known as the *Pliocene Paradox*, (Cronin (2010); Fedorov et al. (2006, 2010)). This paper presents a plausible explanation of the Pliocene paradox~~has been called the *Pliocene Paradox*; see Cronin (2010); Fedorov et al. (2006, 2010). Currently, there is great interest in mid-Pliocene climate as a natural analogue of the future warmer climate expected for Earth, due to anthropogenic forcing. In recent years, significant progress has been achieved in understanding Pliocene climate, for example by: Haywood et al. (2009); Salzmann et al. (2009); Ballantyne et al. (2010); Steph et al. (2010); von der Heydt and Dijkstra (2011); Zhang ; see also references therein. This paper proposes that bistability and bifurcation may have played a fundamental role in determining the Pliocene climate.

The waning of the warm ice-free paleoclimate at the South Pole, leading eventually to abrupt glaciation of Antarctica at the Eocene-Oligocene Transition (EOT) about 34 Ma, is believed to have been caused primarily by two major geological changes (although other factors played a role). One is the movement of the Continent of Antarctica from the Southern Pacific Ocean to its present position over the South Pole, followed by the development of the Antarctic Circumpolar Current (ACC), thus drastically reducing ocean heat transport to the South Pole; see Cronin (2010); Scher et al. (2015). The second is the gradual draw-down in CO_2 concentration world-wide; see DeConto et al. (2008); Goldner, et al. (2014); Pagani et al. (2011). The EBM of this paper includes both CO_2 concentration and ocean heat transport as explicit forcing factors. The results of this paper suggest that the abrupt glaciation of Antarctica at the EOT was the result of a *bifurcation* that occurred as both of these factors changed incrementally; and furthermore, that both are required to explain the abrupt onset of Antarctic glaciation.

In the mid-Cretaceous Period (100 Ma) the climate of the entire Earth was much more *equable* than it is today. This means that, compared to today, the pole-to-equator temperature gradient was much smaller and also the summer/winter variation in temperature at mid to high latitudes was much less (Barron (1983)). The differences in forcing factors between the Cre-

taceous Period and modern times ~~appear~~ appeared to be insufficient to explain this difference in the climates. Eric Barron called this *the warm, equable Cretaceous climate problem* and he ~~studied~~ explored this problem in a series of ~~papers the 1980's (Barron et al. (1981); Barron (1983))~~pioneering papers (Barron et al. (1981); Barron (1983); Sloan and Barron (1992); Barron et al. (1995)). In a similar ~~context~~vein, Huber and Caballero (2011) and Sloan and Barron (1990, 1992) ~~have~~ observed that the early Eocene (56–48 Ma) encompasses the warmest climates of the past 65 million years, yet climate ~~reconstruction studies have failed to reproduce such warm~~ modelling studies had difficulty explaining such warm and equable temperatures. Therefore, this situation ~~has been called the~~ was called the *early Eocene warm equable climate problem*. The ~~present paper presents a mathematical model that gives plausible solutions~~ EBM of the present paper suggests that the mathematical mechanism of *bistability* provides plausible answers to both the ~~Cretaceous~~ mid-Cretaceous and the early Eocene equable climate problems. ~~The key to the solution is that this model, like the actual climate, is *nonlinear* and therefore may exhibit multiple solution states for the same forcing parameters.~~

~~The end of the warm equable climate at the South Pole after the Cretaceous Period, leading eventually to abrupt glaciation of Antarctica about 34 Ma, is believed to have been caused by two major geological changes. One is the movement of the Continent of Antarctica from the Southern Pacific Ocean to its present position over the South Pole, followed by the creation of the Antarctic Circumpolar Current (ACC) , thus drastically reducing ocean heat transport to the South Pole; see Scher et al. (2015). The second is the gradual draw-down in CO_2 concentration world-wide; see DeConto et al. (2008); Goldner, et al. (201 . The EBM~~ In fact, from the perspective of this simple model, these two are mathematically the same problem. Therefore, we call them collectively the *warm equable Paleoclimate problem*. Recent progress in paleoclimate science has succeeded in narrowing the gap between proxy and GCM estimates for the Cretaceous climate (Donnadieu et al. (2006); Ladant and Donnadieu (2016);) and for the Eocene climate (Baatsen et al. (2018); Hutchinson et al. (2018); Lunt et al. (2016, 2017)).

The principal contribution of this paper ~~supports the proposition that both of these mechanisms are required to explain the abrupt Antarctic glaciation.~~

~~The energy balance model presented here is conceptual. It contains many simplifying assumptions and is not intended to give a complete detailed description of the climate of the Earth. It complements, rather than replaces, more detailed General Circulation Models (GCM). This model suggests lines of further research to be carried out with a hierarchy of more sophisticated mathematical models. Such research is already under way and will be reported elsewhere.~~

~~As stated above, a key feature of this family of mathematical models is that they incorporate physical principles that are~~ is a simple climate EBM, based on fundamental physical laws, that exhibits *bistability*, *hysteresis* and *bifurcations*. We propose that these three phenomena have occurred in the paleoclimate record of the Earth and they help to explain certain paleoclimate transitions and puzzles as outlined above. A key property of this EBM is that its underlying physical principles are highly *nonlinear*. As is well known, nonlinear equations can have multiple solutions, unlike linear equations, which can have only one unique solution (if well-posed). In our ~~mathematical models~~EBM, the same set of equations can have two or more co-existing ~~solutions~~stable solutions (bistability), for example an ice-capped solution (like today's climate) and an ice-free solution (like the Cretaceous climate), even with the same values of the forcing parameters. The determination of which solution is actually realized by the planet at a given time is dependent on past history (hysteresis). Changes in forcing parameters may drive

the system abruptly from one stable state to another, at so-called "tipping points". In this paper, these tipping points are investigated mathematically, and are shown to be *bifurcation points*, which ~~can be investigated using *mathematical bifurcation theory*~~are investigated using mathematical bifurcation theory. Bifurcation theory tells us that the existence of bifurcation points is preserved (but the numerical values may change) under small deformations of the model equations. Thus, even though this conceptual model may not give us precise quantitative information about climate changes, qualitatively there is good reason to believe that the *existence* of the bifurcation points in the model will be preserved in similar more refined models and in the real world.

~~Geometrically~~The energy balance model presented here is conceptual and qualitative. It contains many simplifying assumptions and is not intended to give a detailed description of the climate of the Earth with quantitative precision. It complements but does not replace more detailed General Circulation Models (GCM). Very sophisticated GCM, which include many 3D processes, are only able to run a few climate trajectories; while EBM and EMIC may explore more possibilities and investigate climate transitions (tipping points) but with major simplifications. This model suggests lines of further research to be carried out with a hierarchy of more sophisticated models. Geographically, this model is as simple as possible. It follows in a long tradition of *slab models* of the atmosphere. Previous slab models represented the atmosphere of the Earth as a globally-averaged uniform slab at a single temperature T. The temperature T is determined in those models by a global energy balance equation of the form *energy in* = *energy out*. Such models are unable to differentiate between different climates at different latitudes; for example, if the polar climate is changing more rapidly that the tropical climate. In this new model, the forcing parameters of the slab atmosphere are chosen to represent each one of three particular latitudes: Arctic, Antarctic or Tropics. Each of these regions is represented by its own slab model, with its own forcing parameters and its own surface temperature T_S. In addition, each region has its own variable I_A representing the intensity of the radiation ~~emitted~~ re-emitted by the atmosphere. The two independent variables I_A and T_S are determined in each model by two energy balance equations, expressing energy balance in the atmosphere and energy balance at the surface, respectively. In this way, the different climate responses of these three regions to their respective forcings can be explored.

The role played by greenhouse gases in climate change is a particular focus of this model. Greenhouse gases trap heat emitted by the surface and are major contributors to global warming. The very different roles of the two principal greenhouse gases in the atmosphere, carbon dioxide and water vapour, are analyzed here in Sections 2.3.2 and 2.3.3, respectively. The greenhouse warming effect of CO_2 increases with the density of the atmosphere but is independent of temperature, while the greenhouse warming of H_2O increases with temperature but is independent of the density (or partial pressure) of the other gases present. ~~Furthermore, as~~ The greenhouse warming of methane (CH_4) acts in a similar fashion to that of CO_2; therefore, CH_4 can be incorporated in the CO_2 concentration. As an increase in CO_2 concentration causes climate warming, this warming causes an increase in evaporation of H_2O into the atmosphere, which further increases the climate warming beyond that due to CO_2 alone (this is true both in the model and in the real atmosphere). This effect is known as *water vapour feedback*. The energy balance model presented here is the first EBM to incorporate these important roles of the greenhouse gases in such detail.

The paper concludes with two Appendices. In Appendix A, model parameters that are difficult or impossible to determine for paleoclimates are calibrated using the abundant satellite and surface data available for today's climate. In addition, justification

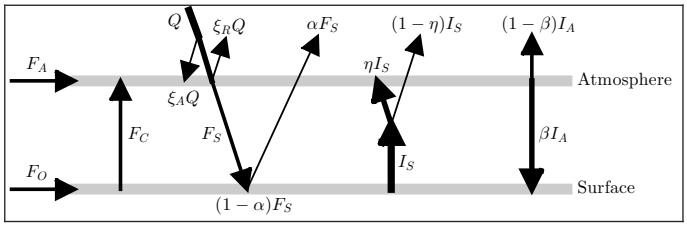

Figure 1. A visualization of the energy balance model. Symbols are defined in Table 1 and Section 2.1.

is given for parameter values chosen for the model. In Appendix B the paleoclimate model of this paper is adapted to modern day conditions and its equilibrium climate sensitivity (ECS) s determined. Here, ECS is the change in global mean temperature produced by a doubling of CO_2 in the model, starting from the pre-industrial value of 270 ppm. For this EBM, the ECS is determined to be $\Delta T = 3.3°C$, which is at the high end of the range accepted by the IPCC, see IPCC (2013).

2 The Energy Balance Climate Model

In this energy balance model (EBM), the atmosphere and surface are each assumed to be in energy balance. ~~The surface layer absorbs short-wave~~ Short-wave radiant energy from the sun ~~, and re-emits~~ is partly reflected by the atmosphere back into space, a small portion is absorbed directly by the atmosphere, and the remainder passes through to the surface. The surface reflects some of this short-wave energy (which is assumed to escape to space) and absorbs the rest, re-emitting long wave radiant energy of intensity I_S, upward into the atmosphere. The atmosphere is modelled as a slab, with greenhouse gases~~that absorb~~, that absorbs a fraction η of the radiant energy I_S from the surface. The atmosphere re-emits radiant energy of total intensity I_A. Of this radiation I_A, a fraction β is directed downward to the surface, and the remaining fraction $(1-\beta)$ goes upward and escapes to space.

This model is based on the uniform slab EBM used in Payne et al. (2015), modified as shown in Figure 1~~and further modified below~~. In our case, the "slab" is a uniform column of air, of unit cross-section, extending vertically above the surface to the tropopause, and located either at a pole or at the equator. The symbols in Figure 1 are defined in Table 1.

This section presents the mathematical derivation of the EBM. Readers interested only in the climate applications of the model may skip this Section and go directly to Section 3. A preliminary version of this EBM was presented in a conference proceedings paper, Dortmans et al. (2017). The present model incorporates several important improvements over that model. The differences between that model and the one presented here are indicated where appropriate in the text. Furthermore, in the previous paper, Dortmans et al. (2017) considered only the application of the model to the Arctic climate and the Pliocene Paradox; it did not study Antarctic or Tropical climate or the Cretaceous Period, as does the present paper.

~~In previous slab models, including Dortmans et al. (2017) and Payne et al. (2015), it was assumed that $\beta = \frac{1}{2}$; that is, the upward and downward radiation intensities from the atmosphere are made equal, see Figure 1. This would be the case for an actual uniform slab; however, the real atmosphere in not uniform in temperature nor density, and in fact both the temperature~~

and density of the atmosphere are much higher in value near the surface than near the tropopause. The net effect of this non-uniformity is that, of the total radiation intensity I_A emitted by the atmosphere, almost two-thirds reaches the surface and only a little more than one-third escapes to space; IPCC (2013). Therefore, in order to have the model in this paper represent the atmosphere more realistically, we choose $\beta = 0.63$ instead of 0.50.

2.1 Energy Balance

The model consists of two energy balance equations, one for the atmosphere and one for the surface. In Figure 1, the so-called *forcings* are shown as arrows, pointing in the direction of energy transfer. These forcings are defined in Table 1. From Figure 1, the energy balance equations for the atmosphere and surface are given respectively by

$$0 \equiv F_A + F_C + \eta I_S - I_A, \quad \text{and}$$
$$0 \equiv F_S - F_C + F_O + \beta I_A - I_S.$$

$$0 = F_A + F_C + \xi_A Q + \eta I_S - I_A, \quad \text{and} \tag{1}$$

$$0 = F_O - F_C + (1-\alpha) F_S - I_S + \beta I_A. \tag{2}$$

Here F_C is the heat transport by conduction/convection from the surface to the atmosphere. For the Arctic model , F_C is assumed negligible; it becomes important only in the Tropics model of Section 3.3Symbols and parameter values for the model are defined in Table 1. Appendix A4 provides derivations and justification for the values of the empirical parameters. The forcings F_O and F_A represent ocean and atmosphere heat transport, respectively. In this model the short wave radiation from the sun F_S passes through the atmosphere without being absorbed. At the surface , the amount of solar radiation absorbed is determined by the , and are specified as constants for each region of interest. Heat transport by conduction/convection from the surface to the atmosphere is denoted F_C. This quantity will be largely dependent on surface temperature, T_S. As described in Appendix A we have modelled it as an hyperbola that is mostly flat for temperatures below freezing, and grows roughly linearly for temperatures above freezing so that

$$F_C = A_1 (T_S - T_R) + \sqrt{A_1^2 (T_S - T_R)^2 + A_2^2}, \tag{3}$$

where A_1 and A_2 are constants. Since the model is concerned with temperatures around the freezing point of water, we set this as a reference temperature, $T_R = 273.15\,\mathrm{K}$.

The annually averaged intensity of solar radiation striking the surface, Q, and by the *albedo* of the surface, α, which is the fraction of a surface parallel to the earth's surface but at the top of the atmosphere is Qreflected by the surface back into space. Thus

$$F_S = (1-\alpha) Q.$$

. The value of Q at either Pole is $Q = 173.2\ \mathrm{Wm}^{-2}$ and at the Equator is $418.8\ \mathrm{Wm}^{-2}$ (McGeehee and Lehman (2012); Kaper and Engler (2013)). Typical values of A fraction ξ_R of this short wave radiation is reflected by the atmosphere back into space

Variables and Parameters Used		
Variables	**Symbol**	**Values**
Mean temperature of the surface	T_S	-50 to +20 C
Infrared radiation from the surface	I_S	141 to 419 W m^{-2}
Mean temperature of the atmosphere	T_A	-70 to 0 C
Energy emitted by the atmosphere	I_A	87 to 219 W m^{-2}
Parameters and Constants	**Symbol**	**Values**
Temperature of freezing point for water	T_R	273.15 K
Stefan-Boltzmann constant	σ	5.670 10^{-8} W m^{-2} K^{-4}
Emissivity of dry air	ϵ	0.9
~~Greenhouse gas absorptivity~~ Fraction of I_A reaching surface	~~η~~ β	~~0 to 1~~ 0.63
~~Absorptivity for CO_2~~ Incident solar radiation	~~η_C~~ Q	~~0 to 1~~ 173.2 W m^{-2} (poles), 418.8 W m^{-2} (equator)
~~Absorptivity for H_2O~~ Fraction of solar radiation reflected from atmosphere	~~η_W~~ ξ_R	~~0~~ 0.2235
Fraction of solar radiation directly absorbed by atmosphere	ξ_A	0.2324
Warm surface albedo	α_W	0.08 to ~~1~~ 0.15
~~Portion of I_A reaching surface~~ Cold surface albedo	~~β~~ α_C	~~0.63~~ 0.7
Albedo transition rate (in tanh function)	$\omega = \Omega/T_R$	0.01
Solar radiation striking surface	F_S	$(1-\xi_R-\xi_A)Q$
Ocean heat transport	F_O	~~20 to 60~~ -55 to 100 W m^{-2}
Atmospheric heat transport	F_A	~~10–127~~ -25 to 45 W m^{-2}
~~Heat transport by conduction / latent heat~~ Vertical heat transport (conduction + evapotranspiration)	F_C	~~0–100 W m^{-2} Absorption of solar radiation F_S $(1-\alpha)Q$ Incident solar radiation at Poles Q_P 173.2~~ 0 to 150 W m^{-2}, function of T_S
~~Incident solar radiation at Equator~~ Vertical heat transport coefficients	~~Q_E~~ a_1, a_2	~~418.8 W m^{-2}~~ 2.650 and 6.590×10^{-2}, respectively
Molar concentration of CO_2 in ppm	μ	270 to ~~600~~ 1600 ppm
Relative humidity of H_2O	δ	~~0 to 1~~ 0.5 to 0.85
~~Absorption coefficient~~ Absorptivity for CO_2	~~k_C~~ η_C	~~0.0474 m^2 kg^{-1}~~ 0 to 1, function of μ
~~Absorption coefficient~~ Absorptivity for H_2O	~~k_W~~ η_W	~~0.0062 m^2 kg^{-1}~~ 0 to 1, function of δ and T_S
~~Warm surface albedo for ocean~~ Absorptivity for clouds	~~α_W~~ η_{Cl}	~~0.08~~ 0.3729
~~Cold surface albedo for Arctic~~ Total atmosphere absorptivity	~~α_C~~ η	~~0.7~~ $1-(1-\eta_W)(1-\eta_C)(1-\eta_{Cl})$
~~Cold surface albedo for Antarctic~~ Grey gas absorption coefficient for CO_2	~~α_C~~ k_C	~~0.8~~ 0.07424 m^2 kg^{-1}
~~Albedo transition rate (in tanh function)~~ Grey gas absorption	~~$\omega = \Omega/T_R$~~	~~0.01~~ 0.05905 m^2 kg^{-1}

and a further fraction ξ_A is directly absorbed by the atmosphere; the remainder penetrates to the surface. See Appendix A1 for the derivation of values for ξ_R and ξ_A. The solar radiation striking the surface of the Earth is

$$F_S = (1 - \xi_R - \xi_A)Q. \tag{4}$$

The surface *albedo* is the ~~albedo~~ fraction, α, of this solar radiation that reflects off the surface back into space. Thus the solar forcing absorbed by the surface is $(1-\alpha)F_S$, and the solar radiation reflected back to space is αF_S. Typical values of the surface albedo α are ~~$0.6-0.9$~~ $0.6--0.9$ for snow, ~~$0.4-0.7$~~ $0.4--0.7$ for ice, 0.2 ~~for cropland and~~ for crop land and 0.1 or less for open ocean.

~~In previous papers, including Dortmans et al. (2017), two discrete values of α are used for polar albedo: a cold albedo α_C for the ice/snow covered surfacebelow the freezing temperature, and a warm albedo α_W corresponding to land or open ocean above the freezing temperature, that is $\alpha =$This discontinuous albedo function is conceptually simple but it is not an accurate representation of what would actually happen if the polar region cooled from ice-free to ice-covered. Recall that this model represents the annually averaged climate. As the polar region cools, there will be a transition period of time in which warm ice-free summers get shorter and cold ice-covered winters get longer. The annually averaged albedo , therefore, would not jump abruptly from low to high constant values as in ; it would transition more smoothly between the summer and winter extreme values. Therefore, in~~ In this paper we introduce a ~~more realistic (and smooth) sigmoidal~~ smoothly varying albedo given by the hyperbolic tangent function~~as in ; see Figure A1.~~ :

$$\alpha(T_S) = \frac{1}{2}\left([\alpha_W + \alpha_C] + [\alpha_W - \alpha_C]\tanh\left(\frac{T_S - 273.15}{\Omega}\,\frac{T_S - T_R}{\Omega}\right)\right)., \tag{5}$$

~~The~~ where α_C and α_W are the albedo values for cold and warm temperatures, respectively, and the parameter Ω determines the steepness of the transition between ~~α_W and~~ α_C and α_W. See Appendix A2 for a full explanation of Equation (5). ~~In this paper, we use $\omega \equiv \Omega/273.15 = 0.01$.~~

~~Subfigure a): Graph of the function tanh(x). Subfigure b): Graphs of the surface energy balance equation using and for α, with $\alpha_c = 0.7$, $\alpha_w = 0.08$ and with $\delta = 0.0$, $\mu = 800$, $F_A = 115$ Wm^{-2} and $\omega \equiv \frac{\Omega}{T_R} = 0.001, 0.01, 0.02, 0.5$, in . There are up to 3 intersections of the blue atmosphere balance equation with the red surface balance equation using , in the figure.~~

The emission of long wave radiation~~from the surface~~ , I, from from a body is governed by the *Stefan-Boltzmann law*, ~~that is~~

$$I_S = \epsilon\sigma T_S^4,$$

~~where $\sigma = 5.670 \times 10^{-8}$ W $\cdot$ m$^{-2} \cdot$ K^{-4}~~ $I = \epsilon\sigma T^4$, where ϵ is the emissivity, σ is the Stefan-Boltzmann constant~~and ϵ is the emissivity, $0 < \epsilon < 1$~~, and T is temperature. The surface of the Earth acts as a black-body, so ~~$\epsilon = 1$ in (6).~~ for the radiation emitted from the surface $\epsilon = 1$, thus

$$I_S = \sigma T_S^4. \tag{6}$$

~~Consider the atmosphere equation of the EBM, that is equation .~~ Previous authors have postulated ~~a~~ an idealized uniform atmospheric temperature T_A for the slab model, ~~satisfying the Stefan-Boltzmann law~~

$$I_A = \epsilon\sigma T_A^4,$$

~~where I_A is~~ so that the intensity of radiation emitted by the atmosphere~~.~~ , I_A, is

$$I_A = \epsilon\sigma T_A^4. \tag{7}$$

The emissivity is $\epsilon = 0.9$ since the atmosphere is an imperfect black-body. ~~Here, T_A is an idealized uniform atmospheric temperature , which~~ A uniform temperature for the atmosphere does not exist in the real world, where T_A varies strongly with height, unlike T_S, which has a single value. Previous two-layer EBMs have used (T_S, T_A) as the two independent variables in the two energy balance equations (1) and (2). ~~However, the value of T_A can not be measured physically, while I_A is a real physical quantity that can be measured with some accuracy. In the present model we choose to avoid use of T_A, and instead~~ Here instead, we use (T_S, I_A) as the two independent variables~~.~~

~~If I_A is the intensity of radiation *emitted* by the atmosphere, then in energy balance (i.e. *energy in = energy out*), the total of all energy *absorbed* by the atmosphere is also equal to~~ , and then we formally let T_A be *defined* by (7). The fraction of I_A ~~, see or . Substituting (4) and (6) into the energy balance equations (1) and (2) gives the following two equations for T_S and I_A.~~

$$\begin{aligned} 0 &\equiv F_A + \eta\sigma T_S^4 - I_A \\ 0 &\equiv (1-\alpha)Q + F_O + \beta I_A - \sigma T_S^4 \end{aligned}$$

~~Here~~ that reaches the surface is $\beta = 0.63$; see Appendix A6.

The parameter η represents the fraction of the ~~radiation $I_S = \sigma T_S^4$~~ infrared radiation I_S from the surface that is absorbed by the atmosphere and is called *absorptivity*. The major constituents of the atmosphere are nitrogen and oxygen and these gases do not absorb any infrared radiation. The gases that do contribute to the absorptivity η are called *greenhouse gases*. Chief among these are carbon dioxide and water vapour. The contribution of these two greenhouse gases to η are analyzed in Sections 2.3.2 and 2.3.3, ~~repectively~~respectively. Although both contribute to warming of the climate, the underlying physical mechanisms of the two are very different. In general, the contribution to η of water vapour is a function of temperature. Another major contributor to absorption is the liquid and solid water in clouds. We model this portion of the absorption as constant, since we do not include any data on cloud cover variation. However, we experimented with making this portion vary with surface temperature, but the results were not qualitatively different than those presented here.

2.1.1 Nondimensional Temperatures

~~In this paper, the temperature is near the freezing point of water , $T_R = 273.15\,^\circ$K.~~ We rescale temperature by ~~this reference temperature~~ the reference temperature $T_R = 273.15$ K and define new nondimensional temperatures and new parameters

$$\tau_A = \frac{T_A}{T_R} \quad \tau_S = \frac{T_S}{T_R} \quad q = \frac{Q}{\sigma T_R^4} \quad f_O = \frac{F_O}{\sigma T_R^4} \quad f_A = \frac{F_A}{\sigma T_R^4} \quad i_A = \frac{I_A}{\sigma T_R^4} \quad \omega = \frac{\Omega}{T_R}.$$

$$\tau_S = \frac{T_S}{T_R}, \quad i_A = \frac{I_A}{\sigma T_R^4}, \quad q = \frac{Q}{\sigma T_R^4}, \quad f_O = \frac{F_O}{\sigma T_R^4}, \quad f_A = \frac{F_A}{\sigma T_R^4}, \quad f_C = \frac{F_C}{\sigma T_R^4}, \quad a_1 = \frac{A_1}{\sigma T_R^3}, \quad a_2 = \frac{A_2}{\sigma T_R^4}, \quad \omega = \frac{\Omega}{T_R}. \tag{8}$$

~~Then~~ After normalization, the freezing temperature of water is represented by $\tau = 1$ and the atmosphere and surface energy balance equations (1)~~or~~ (6) simplify to

$$\begin{aligned} i_A &\equiv f_A + \eta(\tau_S)\tau_S^4 \\ i_A &\equiv \frac{1}{\beta}\left[-(1-\alpha(\tau_S))q - f_O + \tau_S^4)\right], \end{aligned}$$

$$i_A = f_A + f_C(\tau_S) + \xi_A q + \eta(\tau_S)\tau_S^4, \tag{9}$$

$$i_A = \frac{1}{\beta}\left[f_C(\tau_S) - f_O - (1-\alpha(\tau_S))(1-\xi_R-\xi_A)q + \tau_S^4\right], \tag{10}$$

where, from Appendix A

$$f_C(\tau_S) = a_1(\tau_S - 1) + \sqrt{a_1^2(\tau_S-1)^2 + a_2^2}, \tag{11}$$

$$\alpha(\tau_S) = \frac{1}{2}\left([\alpha_W + \alpha_C] + [\alpha_W - \alpha_C]\tanh\left(\frac{\tau_S - 1}{\omega}\right)\right). \tag{12}$$

The range of surface temperatures T_S observed on Earth is ~~actually quite limited; the minimum is well above 0 K and the maximum is well below the boiling~~ restricted to an interval around the freezing point of water, ~~373.15~~273.15 K. ~~Therefore,~~ , and therefore the nondimensional temperature τ lies in an interval around $\tau = 1$. In this paper, we assume ~~$0.6 \le \tau \le 1.3$~~$0.8 \le \tau \le 1.2$, which corresponds approximately to a range in more familiar Celsius degrees of ~~$-100°\mathrm{C} \le T \le +80°\mathrm{C}$~~$-54°\mathrm{C} \le T \le +54°\mathrm{C}$. Another reason for the upper limit on temperature is that the Clausius-Clapeyron Law used in Section 2.3.3 fails to apply at temperatures above the boiling point of water.

2.2 Optical Depth and the Beer-Lambert Law

The goal of this section is to define the absorptivity parameter η in the EBM ~~equation~~ Equation (9) (or (1)~~or~~), in such a way that the ~~greenhouse gases~~ atmosphere in the uniform slab model will absorb the same fraction η of the longwave radiation I_S from the surface as ~~do the corresponding greenhouse gases in the nonuniform real~~ does the real nonuniform atmosphere of the Earth. This absorption is due primarily to water vapour, carbon dioxide, and clouds. Previous energy balance models have assigned a constant value to η, often determined by climate data. In the present EBM, η is not constant but is a function of other more fundamental physical quantities, such as μ, δ, k_C, k_W and T~~; see equations and below~~. This function is determined by classical physical laws. In this way, the present EBM adjusts automatically to changes in these physical quantities, and represents a major advance over previous EBMs.

The Beer-Lambert Law states that when a beam of radiation (or light) enters a sample of absorbing material, the absorption of radiation at any point z is proportional to the intensity of the radiation $I(z)$ and also to the concentration or density of the absorber $\rho(z)$. This bilinearity fails to hold at very high intensity of radiation or high density of absorber, neither of which is the case in the Earth's atmosphere. Whether this Law is applied to the uniform slab model or to the nonuniform real atmosphere, it yields the same differential equation

$$\frac{dI}{dz} = -k\rho(z)I(z), \tag{13}$$

where k ($m^2\,kg^{-1}$) is the absorption coefficient of the material, ρ ($kg\ m^{-3}$) is the density of the absorbing substance such as CO_2, and z (m) is distance along the path. The differential ~~equation~~ Equation (13) may be integrated from $z = 0$ (the surface) to $z = Z$ (the tropopause), to give

$$\frac{I_T}{I_S} = e^{-\int_0^Z k\rho(z)\,dz} \equiv e^{-\lambda}, \quad \text{where} \quad \lambda \equiv \int_0^Z k\rho(z)\,dz. \tag{14}$$

Here $I_T \equiv I(Z)$ is the intensity of radiation escaping to space at the Tropopause $z = Z$, and λ is the so-called *optical depth* of the material. Note that λ is dimensionless. ~~For a mixture of n attenuating materials, with densities ρ_i, absorption coefficients k_i and corresponding optical depths λ_i, the Beer-Lambert Law extends to~~

~~$$\frac{I_T}{I_S} = e^{-\Sigma_{i=1}^n \int_0^Z k_i\rho_i(z)dz} \equiv e^{-\Sigma_{i=1}^n \lambda_i}.$$~~

The absorptivity parameter ~~$\eta = \frac{I_S - I_T}{I_S}$ in equations (1), (??),~~ η in Equations (1) and (9), represents the fraction of the outgoing radiation I_S from the surface that is absorbed by the ~~greenhouse gases in the~~ atmosphere (not to be confused with the absorption coefficient k). It follows from the Beer-Lambert Law that η is completely determined by the corresponding optical depth parameter λ; that is

$$(1-\eta) = \frac{I_T}{I_S} = e^{-\lambda} \text{ or } \eta\frac{I_S - I_T}{I_S} = 1 - e^{-\lambda}. \tag{15}$$

~~Equation~~

For a mixture of n attenuating materials, with densities ρ_i, absorption coefficients k_i and corresponding optical depths λ_i, the Beer-Lambert Law extends to

$$\frac{I_T}{I_S} = e^{-\Sigma_{i=1}^n \int_0^Z k_i\rho_i(z)\,dz} \equiv e^{-\Sigma_{i=1}^n \lambda_i}, \tag{16}$$

so that

$$\eta = 1 - e^{-\Sigma_{i=1}^n \lambda_i} = 1 - \prod_{i=1}^n e^{-\lambda_i} = 1 - \prod_{i=1}^n (1-\eta_i), \qquad \text{where} \qquad \eta_i = 1 - e^{-\lambda_i}. \tag{17}$$

Equation (17) is the key to solving the problem posed in the first sentence of this subsection. For the i^{th} absorbing ~~gas~~ material in the slab model, we set its optical depth λ_i to be equal to the value of the optical depth that this gas has in the Earth's atmosphere as given by (14), and then combine them using (16). This calculation is presented for the case of CO_2 in ~~subsection~~Subsection 2.3.2 and for water vapour in 2.3.3. For the third absorbing material in our model, clouds, we assume a constant value η_{Cl}.

2.3 Greenhouse Gases

The two principal greenhouse gases are carbon dioxide CO_2 and water vapour H_2O. Because they act in different ways, we determine the absorptivities η_C, η_W and optical depths λ_C, λ_W of CO_2 and H_2O separately, and then combine their effects, along with the absorption due to clouds, η_{Cl}, using the Beer-Lambert Law for mixtures,

$$\eta = 1 - (1-\eta_C)(1-\eta_W) = 1 - e^{-\lambda_C - \lambda_W},$$

~~as follows from equation~~ Equation (17). Methane acts similarly to CO_2 and can be included in the optical depth for CO_2. Other greenhouse gases have only minor influence and are ignored in this paper.

2.3.1 The Grey Gas Approximation

Although it is well-known that gases like CO_2 and H_2O absorb infrared radiation I_S only at specific wavelengths (spectral lines), in this paper the *grey gas approximation* is used; that is, the absorption coefficient k_C or k_W is given as a single number averaged over the infrared spectrum, see Pierrehumbert (2010). The thesis Dortmans (2017) presents a survey of values in the literature for the absorption coefficients k_C and k_W of CO_2 and H_2O, respectively, in the grey gas approximation. ~~This work need not be repeated here. The results are shown~~ The values used in this paper are given in Table 1; ~~$k_C = 0.0474\ \mathrm{m^2/kg}$ and $k_W = 0.0062\ \mathrm{m^2/kg}$ are the values used in this paper~~and are derived as described in Appendix A5.

2.3.2 Carbon Dioxide

The concentration of CO_2 in the atmosphere is usually expressed as a ratio, in molar parts per million (ppm) of CO_2 to dry air, and written as μ. There is convincing evidence that μ has varied greatly in the geological history of the Earth, and has decreased slowly over the past 100 million years; however, today μ is increasing due to human activity. The value before the industrial revolution was $\mu = 270$ ppm, but today μ is slightly above 400 ppm.

Although traditionally μ is measured as a ratio of molar concentrations, in practice, both the density ρ and the absorption coefficient k are expressed in mass units of kg. Therefore, before proceeding, μ must be converted from a molar ratio to a ratio of masses in units of kg. The mass of one mole of CO_2 is approximately $mm_C = 44 \times 10^{-3}$ kg/mol. The dry atmosphere is a mixture of 78% Nitrogen, 21% Oxygen and 0.9% Argon, with molar masses of 28 g/mol, 32 g/mol and 40 g/mol, respectively. Neglecting other trace gases in the atmosphere, a weighted average gives the molar mass of the dry atmosphere as $mm_A = 29 \times 10^{-3}$ kg/mol. Therefore, the CO_2 concentration μ measured in molar ppm is converted to mass concentration in kg ppm by multiplication by the ratio $mm_C/mm_A \approx 1.52$. If $\rho_A(z)$ is the density of the atmosphere at altitude z in $\mathrm{kg/m^3}$, then the

mass density of CO_2 at the same altitude, with molar concentration μ ppm, is

$$\rho_C(z) = 1.52\,\frac{\mu}{10^6}\,\rho_A(z) \quad \mathrm{kg/m^3}. \tag{18}$$

It is known that CO_2 disperses rapidly throughout the Earth's atmosphere, so that its concentration μ may be assumed independent of location and altitude, IPCC (2013). As the density of the atmosphere decreases with altitude, the density of CO_2 decreases at exactly the same rate, according to (18). Substituting (18) into (14) determines the optical depth λ_C of CO_2

$$\lambda_C = 1.52\,\frac{\mu}{10^6}\,k_C \int_0^Z \rho_A(z)\,dz. \tag{19}$$

Now consider a vertical column of air, of unit cross-section, from surface to tropopause. The integral in (19) is precisely the total mass of this column~~, $M_A = \int_0^Z \rho_A(z)dz$ (measured in kg, since ρ_A is mass density). This total column mass can be estimated in two independent ways. First, consider the~~ . The atmospheric pressure at the surface ~~, $P_A(0) = 1.013 \times 10^5$ Pa. This is~~ P_A~~,~~ and this is the total weight of the column~~in . Therefore , its total mass is $M_A = P_A(0)/g = 1.033 \times 10^4$, where $g = 9.81$ ms^{-2}~~. Therefore $\int_0^Z \rho(A)\,dz = P_A/g$, where g is acceleration due to gravity. ~~A second determination of the mass M_A of the column of air is as follows. Let $\bar{M} = 5.25 \times 10^{18}$ kg be the total mass of the atmosphere of the Earth and let $\bar{S} = 4\pi R_E^2 = 5.1 \times 10^{14}$ m^2 be the total surface area of the Earth, with radius $R_E = 6.37 \times 10^6$ m. Then the mass of the unit column of atmosphere under consideration here is the mass per unit area; that is, $M_A = \bar{M}/\bar{S} = 1.03 \times 10^4$. These two calculations of M_A agree, up to the second decimal place.~~ Therefore, the optical depth λ_C of CO_2 in the actual atmosphere in (19) is

$$\lambda_C = 1.52\frac{\mu}{10^6}k_C M_A \approx \mu \cdot 7.44 G_C, \qquad \text{where} \qquad G_C \equiv 1.52 \times 10^{-4}~~,^{-6}\, k_C \frac{P_A}{g}. \tag{20}$$

~~where we have used $k_C = 0.0474$ from Subsection 2.3.1. In the slab model, λ_C is chosen to have the same value as for the real atmosphere in .~~ With λ_C so determined, it follows from (15) that

$$\eta_C = 1 - e^{-\lambda_C} = 1 - e^{-\mu \cdot 7.44 \times 10^{-4}} \equiv 1 - \exp(-\mu \cdot G_C), \tag{21}$$

~~where $G_C \equiv 7.44 \times 10^{-4}$ is~~ As listed in Table 1 and derived in Appendix A5, the calibrated value for k_C is 0.07424, and therefore the value for the greenhouse gas parameter for CO_2 ~~, as determined from . Substituting into the EBM equations yields~~

$$i_A \equiv f_A + [1 - \exp(-\mu G_C)] \cdot \tau_S^4,$$

$$i_A \equiv \frac{1}{\beta}\left(\tau_S^4 - [1 - \alpha(\tau_S)]\,q - f_O\right).$$

~~We call this the~~ is $G_C = 1.166 \times 10^{-3}$.

The *dry atmosphere EBM* ~~, because in this case~~ is obtained by assuming there is no water vapour ~~in the model ($\delta = 0$). It is clear that the atmosphereequilibrium equation has a positive y-intercept ($i_A = f_A > 0$ at $\tau_S = 0$), while the surface equation has~~

~~a negative y-intercept ($i_A < 0$ at $\tau_S = 0$). Furthermore, the slope ($\frac{di_A}{d\tau_S}$) of is positive but much less than that of . Therefore, one expects at least one point of intersection of and with positive (τ_S, i_A). However, because of~~ and no clouds in the atmosphere. Hence $\eta = \eta_C$ and $\delta = 0$. We assume also that $\xi_R = \xi_A = 0$. Making these substitutions in the EBM Equations (9)–(10) yields

$$i_A = f_A + f_C(\tau_S) + [1 - \exp(-\mu G_C)] \cdot \tau_S^4, \tag{22}$$

$$i_A = \frac{1}{\beta}\left(f_C(\tau_S) - f_O - [1 - \alpha(\tau_S)]\, q + \tau_S^4\right). \tag{23}$$

Due to the nonlinearity of the ice-albedo ~~term $\alpha(\tau_S)$~~function in (5), there can be in fact up to 3 points of intersection ~~,~~as shown in Figure 2~~ a)~~a. If the CO_2 level μ decreases sufficiently the warm state ($\tau_S > 1$) disappears, while as CO_2 ~~inceases~~ increases the frozen state ($\tau_S < 1$) may disappear. The CO_2 level μ is quite elevated ~~here, because the effect~~ in Figure 2, but the effects of water vapour as a greenhouse gas ~~has~~ and of clouds have been ignored.

Figure 2~~ b)~~b introduces a *bifurcation diagram* (Kuznetsov (2004)), in which the ~~2 EBM equations~~two EBM equations (22)–(23) have been solved for the surface temperature τ_S, which is then plotted as a function of the parameter μ. Figure 2~~ b)~~b shows the 3 distinct solutions τ_S of the EBM: a warm solution ($\tau_S > 1$), a frozen solution ($\tau_S < 1$), and a third solution that crosses through $\tau_S = 1$ and connects the other two solutions in *saddlenode bifurcations* (Kuznetsov (2004)). Stability analysis (Dortmans (2017)) shows that the warm and frozen solutions are *stable* (in a dynamical systems sense), while the third solution (denoted by a dashed line) is unstable.

2.3.3 Water vapour and the Clausius-Clapeyron Equation

In this section, we determine the absorptivity of water vapour as a function of temperature, $\eta_W(\tau_S)$, using fundamental physical laws including the Clausius-Clapeyron ~~Relation~~Equation, the Ideal Gas Law, and the Beer-Lambert Law~~, see Pierrehumbert (2010) , and also assuming~~ ; see Pierrehumbert (2010). We also assume the idealized Lapse Rate of the International Standard Atmosphere (ISA) as defined by ICAO, see ICAO (1993). Unlike CO_2, the concentration of water vapour H_2O in the atmosphere varies widely with location and altitude. This is because the partial pressure of H_2O varies strongly with the local temperature. In fact, it is bounded by a maximum saturated value, which itself is a nonlinear function of temperature, $P_W^{sat}(T)$. The actual partial pressure of water vapour is then a fraction δ of this saturated value,

$$P_W(T) = \delta\, P_W^{sat}(T), \qquad 0 \le \delta \le 1, \tag{24}$$

where δ is called *relative humidity*. While $P_W^{sat}(T)$ varies greatly with T in the atmosphere, the relative humidity δ is ~~more nearly~~ comparatively constant. When the actual $P_W(T)$ exceeds the saturated value $P_W^{sat}(T)$ (i.e. $\delta > 1$), the excess water vapour condenses out of the atmosphere and falls as rain or snow.

The saturated partial pressure at temperature T is determined by the *Clausius-Clapeyron equation*, see Pierrehumbert (2010),

$$P_W^{sat}(T) = P_W^{sat}(T_R) \exp\left(\frac{L_v}{R_W}\left[\frac{1}{T_R} - \frac{1}{T}\right]\right), \tag{25}$$

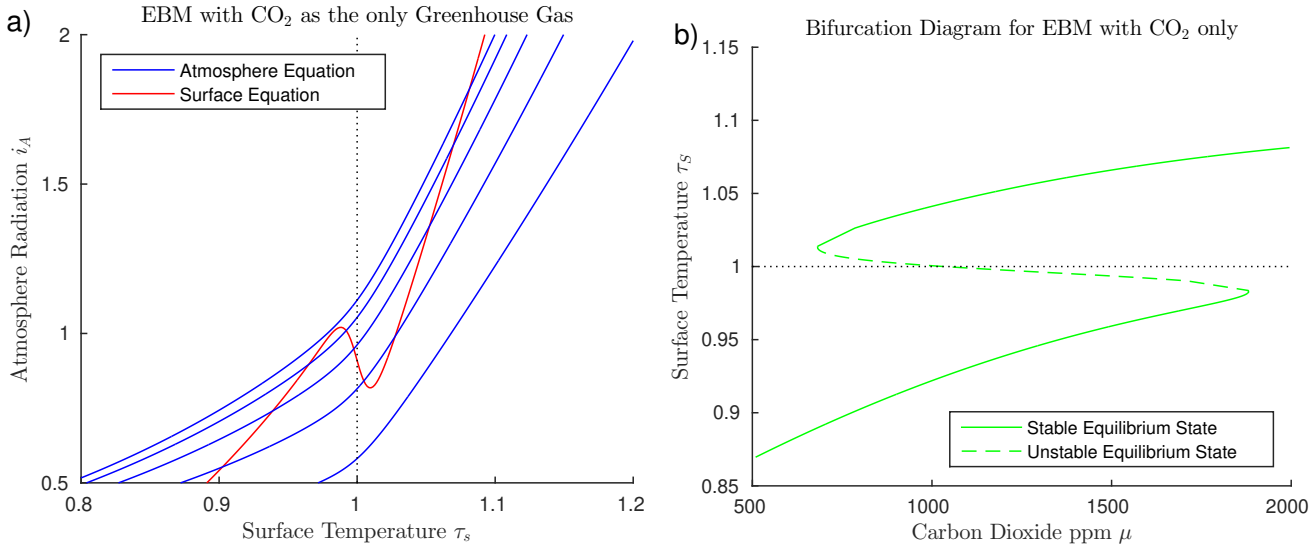

Figure 2. Dry atmosphere EBM (22)–(23) (with ~~$\delta = 0$, $F_A = 115\text{Wm}^{-2}$, $F_O = 36\text{Wm}^{-2}$~~ $F_A = 65$ Wm^{-2}, $F_O = 50$ Wm^{-2}, $Q = 173.2$ Wm^{-2}, $\alpha_W = 0.08$, and $Z = 9$ km). ~~Subfigure~~ a) ~~:~~ CO_2 values ~~$\mu = 2000, 1600, 1200, 800, 400$~~ $\mu = 400, 800, 1200, 1600, 2000$; from ~~top to~~ bottom to top blue curves. A unique cold equilibrium exists for ~~$\mu = 400$~~ $\mu = 400$ (bottom blue curve), multiple equilibria exist for ~~$\mu = 800, 1200, 1600$~~ $\mu = 800, 1200$, and 1600, a unique warm equilibrium exists for $\mu = 2000$ (top blue curve). ~~Subfigure~~ b) ~~:~~ Bifurcation diagram for the same parameters as in a), showing the result of solving the EBM for τ_S as a function of the forcing parameter μ, holding all other forcing parameters constant. Two saddlenode (or fold) bifurcations occur, at approximately ~~$\mu = 600$~~ $\mu = 681$ and ~~$\mu = 1700$~~ $\mu = 1881$. Three distinct solutions exist between these two values of μ. As μ decreases ~~across~~ from right to left in this figure, if the surface temperature starts in the warms state ($\tau_S > 1$) then it abruptly "falls" from the warm state to the frozen state when the left bifurcation point is reached. Similarly, starting on the frozen state ($\tau_S < 1$), if μ increases sufficiently, then the state will jump upward to the warm branch when the right bifurcation point is reached. Both of these transitions are irreversible (one-way).

where T_R is ~~a~~ the reference temperature, here chosen to be the freezing point of water (273.15 K), L_v is the latent heat of vaporization of water and R_W is the ideal gas constant for water, see Table 1. The actual partial pressure of water vapour at relative humidity δ and temperature T is then given by combining equations (24) and (25).

We may use the *Ideal Gas Law* in the form $P_W = \rho_W R_W T$ to convert the partial pressure P_W of water vapour at temperature T to mass density ρ_W of water vapour at that temperature. Substituting into (24) and (25) gives

$$\rho_W(T) = \delta\rho_W^{sat}(T) = \delta\frac{T_R}{T}\rho_W^{sat}(T_R)\frac{P_W^{sat}(T_R)}{R_W T}\exp\left(\frac{L_v}{R_W}\left[\frac{1}{T_R}-\frac{1}{T}\right]\right). \tag{26}$$

Transforming to the dimensionless temperature $\tau = T/T_R$ as in Subsection 2.1.1, this becomes

$$\rho_W(\tau) = \delta\rho_W^{sat}(\tau) = \delta\rho_W^{sat}(1)\left(\frac{P_W^{sat}(T_R)}{R_W T_R}\right)\frac{1}{\tau}\exp\left(\frac{L_v}{R_W T_R}\left[\frac{\tau-1}{\tau}\right]\right). \tag{27}$$

The Beer-Lambert Law in Section 2.2 implies that the absorptivity of a greenhouse gas η_i is completely determined by its optical depth λ_i. For water vapour, from ~~equations and~~Equations (15) and (14),

$$\eta_W = 1 - e^{-\lambda_W} \qquad \text{where} \qquad \lambda_W \equiv \int_0^Z k_W \rho_W(z)\, dz. \tag{28}$$

Here k_W is the absorption coefficient of water vapour; see Appendix A5. In order to evaluate the integral in (28), we need to know how ρ_W varies with height z. We have shown that ρ_W is a function of temperature, given by (26) or (27). Therefore, we need an expression for the variation of temperature T with height z. Under normal conditions, the temperature T decreases with height in the troposphere. This rate of decrease is called the *lapse rate* Γ, and defined as

$$\Gamma \equiv -\frac{dT}{dz}. \tag{29}$$

Normally, Γ is positive and is close to constant in value from the surface to the tropopause. The International Civil Aviation Organization has defined, for reference purposes, the *International Standard Atmosphere* (ISA), in which Γ is assigned the constant value $\Gamma = 6.49 \times 10^{-3}$ K/m, see ICAO (1993). Using this assumption, the variation of temperature with height is given as

$$T(z) = T_S - \Gamma z \quad \text{or} \quad \tau(z) = \tau_S - \gamma z, \tag{30}$$

where the normalized lapse rate is $\gamma = \Gamma / T_R = 2.38 \times 10^{-5}\ m^{-1}$. The tropopause height Z ranges from 8 to 11 km at the poles and 16 to 18 km at the equator, based on satellite measurements; see Kishore et al. (2006). Therefore, both $T(Z)$ and $\tau(Z)$ are positive. For this paper we will take the height to be ~~$Z_P = 9$ km~~ $Z = 9$ km at the poles and ~~$Z_E = 17$ km~~ $Z = 17$ km at the equator.

Equation (30) may be used to change the variable of integration in ~~equation~~ Equation (28), for the optical depth of water vapour, from z to τ. The result is

$$\lambda_W = k_W \int_0^Z \rho_W(\tau(z))\, dz = \frac{k_W}{\gamma} \int_{\tau_S - \gamma Z}^{\tau_S} \rho_W(\tau)\, d\tau. \tag{31}$$

Now substitute (27) into the integral (31) and simplify to

$$\lambda_W(\tau_S) \;=\; \delta\, G_{W2} \int_{\tau_S - \gamma Z}^{\tau_S} \frac{1}{\tau} \exp\left(G_{W1} \left[\frac{\tau - 1}{\tau} \right] \right) d\tau, \tag{32}$$

where the greenhouse gas ~~constants~~ parameters G_{W1} and G_{W2} for water vapour are defined as

$$G_{W1} \equiv \frac{L_v}{R_W T_R} = 17.90 \quad \text{and} \quad G_{W2} \equiv \frac{k_W \rho_W^{sat}(1)}{\gamma} = 1.265 \frac{k_W P_W^{sat}(T_R)}{R_W T_R \gamma}. \tag{33}$$

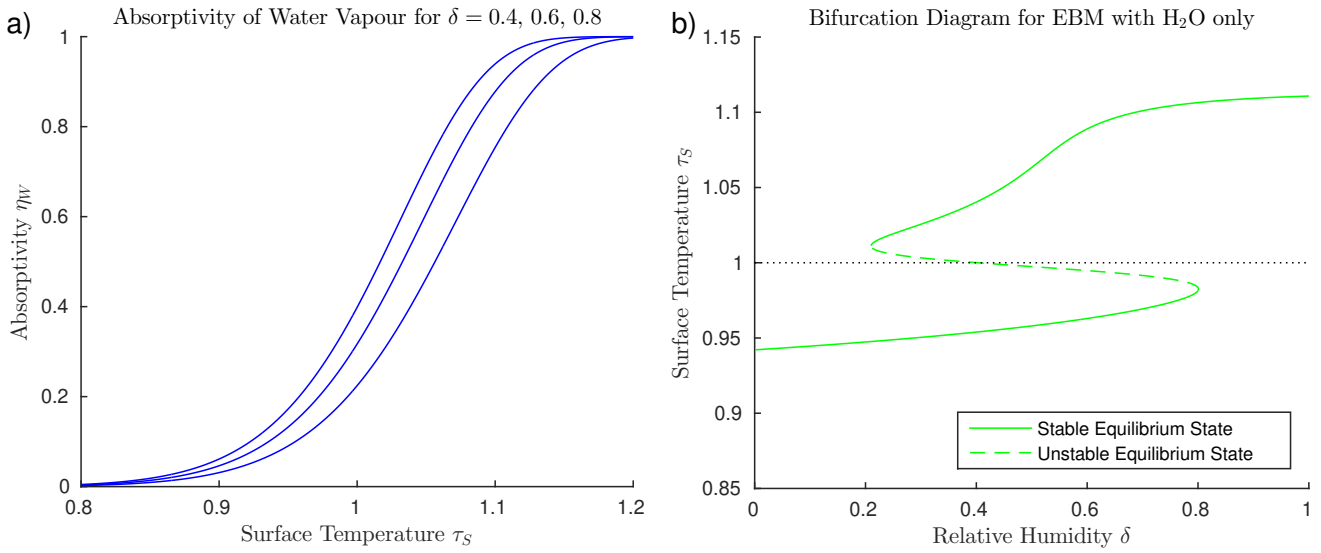

Figure 3. ~~Greenhouse~~ Climate EBM (9)~~–~~(10) including greenhouse effect of Water Vapour only, $\mu = 0$ (~~$\mu = 0$~~with $F_A = 45\ \mathrm{Wm}^{-2}$, $F_O = 50\ \mathrm{Wm}^{-2}$, $Q = 173.2\ \mathrm{Wm}^{-2}$, $\alpha_W = 0.08$, and $Z = 9$ km). ~~Subfigure~~ a) ~~:~~ Absorptivity $\eta_W(\tau_S)$ as given by ~~equation~~ Equation (34) with ~~$\delta = 0.6,\ 0.4,\ 0.2$~~ relative humidity $\delta = 0.4,\ 0.6,\ 0.8$, from ~~top to~~ bottom to top blue lines. Below freezing ~~,~~(~~$\tau_s < 1$,~~)~~ water vapour has ~~very~~ little influence as a greenhouse gas, but absorptivity increases rapidly to approach $\eta = 1$ for $\tau > 1$. ~~Subfigure~~ b) ~~: Atmosphere energy balance equation~~ Bifurcation diagram for EBM with $\mu = 0$, and relative humidity ~~values $\delta = 0.7,\ 0.5,\ 0.3,\ 0.1$,~~ increasing from ~~top~~ 0 to ~~bottom blue lines. There is little greenhouse effect for $\tau_S < 1$ but~~ 1. Note the ~~greenhouse warming effect for $\tau_S > 1$ increases strongly with~~ accelerated increase in surface temperature τ_S ~~and with δ~~above $\tau_S = 1$, compared to that in Figure 2b, due to the rapid increase in η_W.

Finally, using the Beer-Lambert Law, the absorptivity η_W of water vapour in ~~equation~~ Equation (28) is determined by its optical depth, and is now a function of the surface temperature,

$$\eta_W(\tau_S) = 1 - \exp\left[-\lambda_W(\tau_S)\right] = 1 - \exp\left[-\delta\, G_{W2} \int_{\tau_S - \gamma Z}^{\tau_S} \frac{1}{\tau} \exp\left(G_{W1}\left[\frac{\tau - 1}{\tau}\right]\right) d\tau\right]. \tag{34}$$

The definite integral in this expression is easily evaluated numerically in the process of solving the atmosphere and surface EBM equations. As given in Table 1 and derived in Appendix A5, the calibrated value of k_W is $0.05905\ \mathrm{m}^2\ \mathrm{kg}^{-1}$ and the greenhouse gas parameters for H_2O are

$G_{W1} = 17.89$ and $G_{W2} = 12.05$.

Figure 3~~(a)~~ a shows that the function $\eta_W(\tau_S)$ in (34) increases rapidly from near 0 to near 1 as τ_S increases past 1, and it steepens towards a step function as δ increases. This implies that, if the surface temperature τ_S in the surface energy balance ~~equation~~ Equation (10) increases past $\tau_S = 1$, then the absorptivity of water vapour $\eta_W(\tau_S)$, acting as a greenhouse gas in ~~equation~~ Equation (9), increases rapidly, thus amplifying the heating of the atmosphere by the radiation $I_S = \sigma T_S^4$ from

the surface. Energy balance requires a corresponding increase in the radiation I_A transmitted from the atmosphere back to the surface, further increasing the surface temperature τ_S. This is a positive feedback loop called *water vapour feedback*. This positive feedback is manifested in Figure 3~~shows two views of this dramatic water vapour feedback effect.~~ b in the additional increase in T_S on the warm branch, beyond that due to the ice-albedo bifurcation. Compare this with Figure 2, where no water vapour is present. This rapid nonlinear change is due to the relatively large size of the greenhouse constant ~~$G_{W1} = \frac{L_v}{R_W T_R} = 17.9$~~$G_{W1} = \frac{L_v}{R_W T_R} = 17.89$, in the exponent of the Clausius-Clapeyron ~~equation~~ Equation (27), as it reappears in ~~equation~~ Equation (34).

2.3.4 Combined CO_2 and H_2O Greenhouse Gases

The combined effect of two greenhouse gases is determined by the Beer-Lambert Law as shown in Section 2.2. If η_C is the absorptivity of CO_2 as in (21) and η_W is the absorptivity of H_2O as in (28), then the combined absorptivity ~~η_{CW} of the~~ η of these two is obtained by adding the two corresponding optical depths λ_C and λ_W. The overall absorptivity of the atmosphere including these two greenhouse gases and the (assumed) constant effect of clouds is, by (17),

~~$$\eta_{CW}(\tau_S) = 1 - \exp\left[-\lambda_C - \lambda_W(\tau_S)\right] = 1 - \exp\left[-\mu \cdot G_C - \delta\, G_{W2} \int_{\tau_S - \gamma Z}^{\tau_S} \frac{1}{\tau} \exp\left(G_{W1}\left[\frac{\tau - 1}{\tau}\right]\right) d\tau\right],$$~~

$$\eta(\tau_S) = 1 - (1-\eta_C)(1-\eta_W)(1-\eta_{Cl}) = 1 - \exp\left[-\lambda_C - \lambda_W(\tau_S)\right](1-\eta_{Cl})$$
$$= 1 - \exp\left[-\mu \cdot G_C - \delta\, G_{W2} \int_{\tau_S - \gamma Z}^{\tau_S} \frac{1}{\tau} \exp\left(G_{W1}\left[\frac{\tau - 1}{\tau}\right]\right) d\tau\right](1-\eta_{Cl}). \tag{35}$$

~~After these substitutions the~~ The full nondimensional two-layer EBM ~~equations become~~

$$i_A \equiv f_A + \eta_{CW}(\tau_S) \cdot \tau_S^4,$$
$$i_A \equiv \frac{1}{\beta}\left(\tau_S^4 - [1-\alpha(\tau_S)]\, q - f_O\right).$$

~~where $\alpha(\tau_S)$ is defined in equation , $\eta_{CW}(\tau_S)$ is defined in equation~~ is therefore specified by Equations (9)–(12) and (35), and the ~~remaining parameters are given~~ parameter values in Table ~~1. Note that the atmosphere radiation variable i_A is easily eliminated from equations , leaving a single equation for the unknown equilibrium surface temperature τ_S,~~

$$0 = [1-\alpha(\tau_S)]\, q + f_O + \beta f_A - [1 - \beta\eta_{CW}(\tau_S)]\, \tau_S^4.$$

~~This form of the EBM is useful for obtaining bifurcation diagrams~~1.

2.4 Positive Feedback Mechanisms

The above analysis shows that there are two highly nonlinear positive ~~feedbacks~~ feedback mechanisms in this EBM. Both serve to amplify an increase (or decrease) in surface temperature T_S near the freezing point, as follows. Consider the case of rising

temperature~~, near the freezing point~~. The first feedback is ~~due to~~ *ice-albedo feedback*, due to a change in albedo in the surface equilibrium equation. As illustrated in Figure A1, if the surface temperature increases slowly ~~thought~~ through the freezing point, causing a drop in albedo, there is a large increase in solar energy absorbed, leading to an abrupt increase in temperature. The second is ~~water vapour feedback~~ *water vapour feedback* in the atmosphere equilibrium equation~~,~~. As shown in Figure 3~~. If~~ , if the surface temperature continues to increase above freezing, then the absorptivity of water vapour increases dramatically, ~~adding energy to the system~~ strengthening the greenhouse effect for water vapour and further increasing the temperature. Both of these ~~forcings are called positive feedbacks, because they amplify the warming effect of the original forcing~~mechanisms act independently of the concentration of CO_2 itself in the atmosphere. However, if the concentration of CO_2 goes up, causing a rise in temperature, then each of these two positive feedback mechanisms can *amplify* the increase in temperature that would occur due to CO_2 alone.

3 Applications of the Energy Balance Model

The goal of this section is an exploration of the underlying causes of abrupt climate changes that have occurred on Earth in the past 100 million years, using as a tool the EBM developed in Section 2. The most dramatic climate changes occurred in the two polar regions of the Earth. The climate of the tropical region of the Earth has changed relatively little in the past 100 million years. In ~~mathematics, a nonlinear system can have multiple solution states coexisting at the same parameter values. A small change in the parameters may cause a solution of the system to jump from one state to another, with very different characteristics. Mathematical bifurcation theory is useful for detecting and explaining such multiple states and transitions.~~

~~In~~ this Section, the ~~EBM is~~ EBMs for the two polar regions are applied to the Arctic Pliocene Paradox, the glaciation of Antarctica, the ~~Pliocene Paradox, the~~ warm equable Cretaceous problem and the warm equable Eocene problem. For comparison, a control EBM with parameter values set to those of the Tropics shows no abrupt climate changes in the Tropical climate for the past 100 million years.

3.1 ~~EBM for the Glaciation of Antarctica~~

~~Antarctica in the mid-Cretaceous Period was ice-free, and it remained so for the remainder of the Cretaceous Period and well into the Paleogene (65 – 23 Ma). In the mid-Cretaceous, the continent of Antarctica was in the South Pacific Ocean. At that time, the South Pole was located in open ocean and was warmed by Pacific Ocean currents, as was Antarctica. However, the continent of Antarctica moved poleward and began to encroach upon the South Pole towards the end of the Cretaceous, fully covering the South Pole by the end of the Eocene, see Briggs (1987). The diminishing marine influence on the South Pole coincided with the onset of cooling of Antarctica about 45 Ma (mid-Eocene). The opening of the both the Drake Passage (between South America and Antarctica) and of the Tasmanian Gateway (between Antarctica and Australia) near the end of the Eocene (34 Ma), led to the creation of the Antarctic Circumpolar Current (ACC), which further isolated the South Pole from warm ocean heat transport and accelerated the cooling and glaciation of Antarctica; Cronin (2010). Therefore, from the early Eocene to the late Oligocene, the ocean heat transport to the South Polar region decreased significantly, from near the Cretaceous value, about~~

100 Wm^2 (Barron et al. (1981)), to a much lower value, taken here to be 30 Wm^2. The geological record shows an abrupt drop in temperature and the onset of massive glaciation in Antarctica, at the Eocene-Oligocene boundary, about 34 MYa.

Because the atmosphere is well mixed, at any given time the CO_2 level in the Antarctic is the same as worldwide. Estimates of Eocene CO_2 concentration μ vary widely. For example Pagani et al. (2005, 2006) estimate Eocene CO_2 concentration at 1000-1500 ppm, while Wolfe et al. (2017) estimate 490 ppm. For this EBM, we estimate early Eocene global CO_2 level as $\nu = 1100$ ppm. According to Pagani et al. (2005, 2006); Cronin (2010); this had decreased to approximately modern levels by the end of the Oligocene, 23 Ma, that is to $\mu = 400$ ppm.

In the recent literature, there has been a vigorous discussion of whether the primary cause of the onset of Antarctic glaciation is the slow decline in CO_2 concentration, or the decrease in poleward ocean heat transport due to the opening of ocean gateways and the creation of the ACC; see DeConto et al. (2008); Goldner, et al. (2014); Pagani et al. (2011); Scher et al. (2015). In the work of Scher et al. (2015), it is observed that onset of the ACC coincided with major changes in global ocean circulation, which probably contributed to the drawdown in CO_2 concentration in the atmosphere. Since both CO_2 concentration and ocean heat transport F_O are explicit parameters in the EBM presented here, they can be varied independently in the model to investigate which one played a primary role.

EBM for the Glaciation of Antarctica. Subfigure a): Graphs of EBM equations, with F_O fixed at 80 Wm^{-2} in the surface equation (red line), and with CO_2 concentration μ in the atmosphere equation decreasing (from top to bottom blue lines) $\mu = 1500, 1200, 900, 600, 300$ ppm. Subfigure b): Graphs of the same EBM equations, but with CO_2 concentration μ fixed at 1100 ppm (blue line) and with ocean heat transport F_O decreasing (from bottom to top red lines) 80, 60, 40, 20, 0 Wm^{-2}.

Figure 5 shows the solutions of the EBM equations for Antarctic parameter values, including $F_A = 52$ Wm^{-2}. Points of intersection of one red line (surface equation) and one blue line (atmosphere equation) are the equilibrium solutions of the system. In general, there can be up to three solutions: a frozen solution (with $\tau_S < 1$), a warm solution (with $\tau_S > 1$), and an intermediate solution, on the downward sloping portion of the red line, which is unstable in the dynamical systems sense. (The other two solutions are always stable, see Dortmans (2017).) In Figure 5 a) the ocean heat transport F_O in held fixed, while CO_2 concentration μ is decreased, from the top to bottom blue lines. In Figure 5 b) the reverse is true; the CO_2 concentration μ is held fixed while the ocean heat transport F_O is decreased, from bottom to top red lines. In each case, for a sufficiently small value of μ or F_O, respectively, the warm solution disappears. This occurs when the warm solution meets the unstable intermediate solution. When the two meet, they coalesce then disappear, in what is called a *saddlenode bifurcation* in dynamical systems theory (Kuznetsov (2004)). Beyond this bifurcation, only the frozen solution ($\tau_S < 1$) exists.

Figure 6 displays *bifurcation diagrams*, in which the surface temperature τ_S, which has been determined as a solution of the EBM, is plotted while parameters in the EBM are varied smoothly, from the early Eocene values, 55 million years ago, to the late Oligocene values, 23 million years ago. These dates are chosen to bracket the time of the glaciation of Antarctica. First we introduce a *bifurcation parameter* ν, which acts as a surrogate time variable. The bifurcation parameter ν is related to geological time by

$$t = 55 - 32 \cdot \nu \quad \mathrm{Ma.}$$

Thus, $\nu = 0$ corresponds to the early Eocene 55 Ma and $\nu = 1$ corresponds to the late Oligocene 23 Ma. During this time, it is known that both CO_2 concentration μ and ocean heat transport F_O were decreasing slowly. To study the effects of the simultaneous reduction of μ and F_O, we express both as simple linear functions of the bifurcation parameter ν, as follows:

$$\begin{aligned} \mu &\equiv 1100 - 700 \cdot \nu, \\ F_O &\equiv 100 - 70 \cdot \nu, \qquad 0 \le \nu \le 1. \end{aligned}$$

Here, $\nu = 0$ corresponds to the high early Eocene values of $\mu = 1100$ and $F_O = 100$, while $\nu = 1$ corresponds to the low Oligocene-Miocene boundary values of $\mu = 400$ and $F_O = 30$. Thus, in equations , as ν increases from 0 to 1, the climate forcing factors μ and F_O decrease linearly from their Eocene values to late Oligocene values. Strictly speaking, these forcings did not change linearly in time; however, the decease is fairly close to linear, and for qualitative results we can make this simplifying assumption in the EBM. The parameter F_A is held constant at $F_A = 52$, from Barron et al. (1981). Albedo for the fresh snow in Antarctica is $\alpha_C = 0.8$. Other parameters are as in Table 1.

Figure 6 a) shows a saddlenode bifurcation at $\nu = 0.606$, corresponding to forcing parameter values $\mu = 676$ ppm and $F_O = 57.6\,\mathrm{Wm}^{-2}$ in the model, and to geological time about 35 Ma, assuming the linear time relation in . This corresponds remarkably closely to best estimates of the timing of glaciation in the geological record of about 34 Ma. The warm state and frozen state temperatures coexisting at the bifurcation point are $+4.6°\mathrm{C}$ and $-40.2°\mathrm{C}$. These temperatures are close to paleoclimate estimates (Cronin (2010)). As ν increases past the bifurcation point $\nu = 0.606$, the warm climate state ceases to exist, and the climate system transitions ("falls") rapidly, from the saddlenode point to the frozen state, Kuznetsov (2004). Thus the EBM reproduces the abrupt transition to the glaciation of Antarctica, which is seen in the geological record.

Bifurcation Diagrams for the Glaciation of Antarctica. Subfigure a): This shows a saddlenode bifurcation at $\nu = 0.606$, corresponding to forcing parameter values $\mu = 676$ ppm and $F_O = 57.6\,\mathrm{Wm}^{-2}$ in equations . As ν increases through this saddlenode bifurcation point, the climate will transition abruptly from a warm state to a frozen state. The warm state and frozen state temperatures coexisting at the bifurcation point are $+4.6°\mathrm{C}$ and $-40.2°\mathrm{C}$. The bifurcation point corresponds to a geological time of about 35 Ma, assuming the linear model equations . Subfigure b): Two superimposed bifurcation diagrams as in a), except that, on the green curves, F_O is held fixed at its Eocene values while μ deceases as in , and on the yellow curves, μ is held fixed at the Eocene value while F_O decreases as in . No saddlenode bifurcation occurs in either scenario.

Figure 6 b) explores the relative importance of decreasing CO_2 concentration μ and decreasing ocean heat transport F_O in the glaciation of Antarctica. The green curves represent a scenario in which μ decreases as in equation but F_O is held fixed at its Eocene value, and the yellow curves represent a case in which μ is held fixed at its Eocene value while F_O decreases according to . In neither case does a glaciation event occur. The analysis of this paper implies that significant decreases in *both* CO_2 concentration μ and ocean heat transport F_O are required to achieve a saddlenode bifurcation, and the observed transition to a frozen Antarctic state.

While the glaciation of Antarctica is an accepted fact in paleoclimate science, the suddenness of the climate change that occurred in Antarctica near the Eocene-Oligocene boundary (33.9 Ma), a time when the forcing parameters were changing slowly, has not been adequately explained. The bifurcation analysis presented here presents a simple but plausible explanation

~~that fills this gap in the literature. Furthermore, this EBM supports the hypothesis that *both* falling CO_2 concentration μ and decreasing ocean heat transport F_O are essential to an explanation of the sudden glaciation of Antarctica.~~

3.1 EBM for the Pliocene Paradox

The Arctic region of the Earth's surface has had ice cover year-round for only the past few million years. For at least 100 million years prior to about ~~5~~ 3 Ma, the Arctic had no permanent ice cover, although there could have been seasonal snow in the winter. Recently, investigators have found plant and animal remains, in particular on the farthest northern islands of the Canadian Arctic Archipelago, which demonstrate that there ~~once~~ was a wet temperate rainforest there for millions of years, similar to that now present on the Pacific Northwest coast of North America; see ~~Basinger et al. (1994); Greenwood et al. (2010); Jahren and Sternberg (2003);~~ Basinger et al. (1994); Greenwood et al. (2010); Struzik (2015); West et al. (2015); Wolfe et al. (2017). The relative humidity has been estimated at 67% by Jahren and Sternberg (2003), and this value has been chosen for δ in the Arctic EBM of this section. The change from ice-free to ice-covered in the Arctic occurred abruptly, during the Pliocene Epoch, 5.3 to 2.6 Ma. It has been a longstanding challenge ~~for paleoclimatologists~~ to explain this dramatic change in the climate.

~~During the Pliocene Epoch, all of the~~ Currently, there is great interest in the mid-Pliocene climate, because it is the most recent paleoclimate that resembles the future warmer climate now predicted for the Earth. Significant progress in understanding Pliocene climate has been achieved in recent years. The Pliocene Research, Interpretation and Synoptic Mapping (PRISM) project of the US Geological Survey has contributed to this goal, see Dowsett et al. (2011, 2013, 2016), as has the Pliocene Model Intercomparison Project (PlioMIP), see Haywood et al. (2011, 2016); Zhang et al. (2013). Advances in the extraction and interpretation of proxy data have given a clearer picture of the warm Pliocene climate, see Haywood et al. (2009); Salzmann et al. (2009 . At the same time, computer models have achieved closer agreement with proxy data, see for example Haywood et al. (2009); Dowsett et al ; nd other references therein. Using a fully coupled Atmosphere-Ocean GCM, Lunt et al. (2008) considered the following forcing factors contributing to late Pliocene glaciation: decreasing carbon dioxide concentration, closure of the Panama seaway, end of a permanent El Niño state, tectonic uplift and changing orbital parameters. They concluded that falling CO_2 levels were primarily responsible for the formation of the Greenland ice-sheet in the late Pliocene.

During the Pliocene Epoch, important forcing factors that determine climate were very similar to those of today. The Earth orbital parameters, the CO_2 concentration, solar radiation intensity, position of the continents, ocean currents and atmospheric circulation all had values close to the values they have today. Yet, in the early~~Pliocene, 4–5~~ /mid Pliocene, 3.5–5 million years ago, the Arctic climate was much milder than that of today. Arctic surface temperatures were $8 - -19°C$ warmer than today and global sea levels were $15 - -20$ m higher than today, and yet CO_2 levels are estimated to have been $340 - -400$ ppm, about the same as 20th Century values; see Ballantyne et al. (2010); Csank et al. (2011); Tedford and Harington (2003). As mentioned in the Introduction, the problem of explaining how such dramatically different climates could exist with such similar forcing parameter values has been called the *Pliocene Paradox* (Cronin (2010); Fedorov et al. (2006, 2010); Zhang and Yan (2012)).

Another interesting ~~paradox~~ fact concerning Polar glaciation is ~~the fact~~ that, although both poles have transitioned abruptly from ice-free to ice-covered, they did so at very different geological times. The climate forcing conditions of Earth are highly

symmetric between the two hemispheres, and for most of the ~~history of Earth~~ past 200 million years (or more) the climates of the two poles have been ~~very~~ similar. However, there was an anomalous ~~period~~ interval of about 30 million years, from the Eocene-Oligocene ~~boundary (~~Transition (EOT) 34 Ma~~),~~ , to the early Pliocene ~~(~~4 Ma~~),~~, when the Antarctic was largely ice-covered but the Arctic was ~~ice-free.~~ largely land ice free. Because CO_2 disperses rapidly in the Atmosphere, its concentration μ must be the same everywhere, at any given time. Therefore we seek a forcing factor other than μ to account for this 30 million year period of broken symmetry. One obvious difference is geography. Since the Eocene, the South Pole has been land-locked in Antarctica, while the North Pole has been in the Arctic Ocean. Therefore, our two EBMs for the North and South Poles have very different values for ocean heat transport F_O. We will show that this difference is sufficient to account for the gap of 30 million years between the Antarctic and Arctic glaciations.

~~An important feature of Arctic climate in the early Pliocene, and for many millions of years earlier, was that the relative humidity δ was much higher than today. The~~ Our Pliocene Arctic EBM brackets the Pliocene Epoch between the mid-Eocene ~~climate has been described as a wet temperate rainforest (Greenwood et al. (2010)), with estimated relative humidity of 67% (Jahren and Sternberg (2003)), and these conditions prevailed with only minor fluctuations until the Pliocene. For this Arctic EBM, we choose $\delta = 0.67$. Important nonlinear physical relationships among the temperature, the water vapour pressure, the water vapour greenhouse heating effect and the relative humidity, were explored in Subsection 2.3.3 and incorporated into the EBM there~~(50Ma) and pre-industrial modern times, and it models the effects of the slow decrease in both CO_2 and ocean heat transport F_O in the Arctic, over this long time interval. In this Arctic model, abrupt glaciation of the Arctic is inevitable, due to the existence of a bifurcation point.

During the Eocene (56 – 34 Ma), ~~global~~ temperatures were much higher than today, ~~particularly~~ especially in the Arctic (Greenwood et al. (2010); Wolfe et al. (2017); Huber and Caballero (2011)), ~~with~~ and CO_2 concentration μ ~~and ocean heat transport to the Arctic F_O also~~ also was higher than today~~, and decreased slowly to today's values over geoloical time scales.~~ . Estimates of Eocene CO_2 concentration μ vary, from 1000–1500 ppm (Pagani et al. (2005, 2006)), to 490 ppm (Wolfe et al. (2017)). For this EBM, we set mid-Eocene CO_2 at $\mu = 1000$ (Pagani et al. (2005)). ~~The~~ Both temperature and CO_2 concentration have decreased steadily but not monotonically, with many fluctuations, from their Eocene values to pre-industrial modern values. The overall decrease in CO_2 concentration observed since the Eocene may be attributed to ~~deceased~~ decreased volcanic activity, increased absorption and sequestration by vegetation ~~,~~and the oceans, continental erosion and other sinks.

The changes in ocean heat transport to the Arctic are more complicated and derive from many factors only summarized here; see De Schepper et al. (2015); Haug et al. (2004); Knies et al. (2014); Lunt et al. (2008); Zhang et al. (2013). There was a slow drop in global sea level, in large part due to the gradual accumulation of vast amounts of water in the form of ice and snow on Antarctica. It has been estimated that the total amount of ice today in the Antarctic is equivalent to a change in sea level of about 58 m (Fretwell et al. (2013); IPCC (2013)). This drop in sea level likely reduced the flow of warm ~~surface~~ tropical ocean water into the Arctic. ~~However, other factors were at play~~Against this background, several other factors came into play, due to changing geography. In the Eocene, the North Atlantic Ocean ~~did not yet exist~~was not always connected to the Arctic, but the Turgai ~~Strait~~ Sea existed between Europe and Asia and connected the warm Indian Ocean to the Arctic, until about 29 Ma (Briggs (1987)). By the ~~Miocene, The Turgai Strait~~ Oligocene, the Turgai Sea had closed and the North Atlantic had opened

between Greenland and Norway, forming a deep-water connection to the Arctic Ocean. The Bering Strait opened and closed. During the Pliocene the formation of the Isthmus of Panama about 3.5 Ma cut off ~~an~~ a warm equatorial current that had existed between the ~~warm Atlantic and cooler~~ Atlantic and Pacific, at least since Cretaceous times. On the Atlantic side of the Isthmus, the sea water became warmer, and became more saline due to evaporation. The Gulf Stream carried this warm salty water to Western Europe. One might expect the Gulf Stream to transport more heat into the Arctic. However, some believe that the Gulf Stream actually contributed to glaciation in the Arctic, as follows (Haug et al. (2004); Bartoli et al. (2005)). Evaporation from the Gulf Stream waters contributed to rainfall across Northern Europe and Siberia, increasing the flow of fresh water in rivers emptying into the Arctic Ocean. This reduced the salinity, and hence the density, of the Arctic Ocean waters. The Gulf Stream waters in the North Atlantic, now cooler, and denser due to high salinity, were forced downward by the less dense Arctic waters, ~~and then~~ which began to flow into the North Atlantic on the surface. The denser Gulf Stream waters returned southward as a deep ocean current, without having conveyed much heat to the Arctic. Meanwhile the low salinity Arctic surface water, with a higher freezing temperature, began to freeze, resulting in higher albedo and accelerating Arctic glaciation. In large measure, these changing geographical factors partially cancelled each other in their contributions to ocean heat transport to the Arctic. In the EBM, we summarize all of the above heat transport mechanisms by specifying a slow overall decrease in ocean heat transport to the Arctic, represented by the single forcing parameter F_O. ~~As explained above, the net decrease in F_O is small.~~

Figure 4 ~~a)~~ a shows graphs of the surface and atmosphere equilibrium equations for the Arctic Pliocene EBM, for varying values of μ. ~~We do not show a figure with decreasing ocean heat transport F_O, analogous to Figure 5 b), because the decrease~~ The figure shows only one surface equilibrium curve (red), with $F_O = 50\ \mathrm{Wm}^{-2}$, because the change in F_O is relatively small~~in the Arctic. Again, it~~. The blue atmosphere equilibrium curves represent values of CO_2 concentration μ falling from 1100 to 200 ppm, from the top to bottom blue curves. It is clear that there may exist up to 3 points of intersection of a given atmosphere equilibrium curve (blue) with ~~a~~ the surface equilibrium curve (red); namely, a warm equilibrium state ~~$\tau_s > 0$~~ $\tau_s \gg 1$, a frozen equilibrium state ~~$\tau_S < 0$~~ $\tau_S < 1$, and a third (intermediate) solution, which is always unstable (when it exists). ~~Just as in Figure 5, as~~ As μ decreases and the warm equilibrium state $\tau_s > 1$ approaches the local minimum on the red S-curve~~,~~; at the same time the unstable intermediate equilibrium state moves down the middle branch of the red S-curve. When they meet, these two equilibria coalesce, then disappear, via a saddlenode bifurcation. Beyond this saddlenode bifurcation, only one equilibrium state remains, that is the stable frozen state on the left in the Figure. Dynamical systems theory tells us that following this bifurcation, the system will transition rapidly to that frozen equilibrium state. The paleoclimate record shows that ~~both~~ CO_2 concentration ~~and ocean heat transport F_O were~~ was trending downward for millions of years before and during the Pliocene. Therefore, Figure 4 ~~a)~~ a predicts that an abrupt drop in temperature to a frozen state would be inevitable, if this trend continued far enough.

In order to explore this downward trend further, we bracket the Pliocene Epoch between the mid-Eocene Epoch (50 Ma) and the pre-industrial modern era (300 years ago), and define a surrogate time variable ν ~~(as in Section 3.2)~~ by

$$t = 50(1-\nu) \quad \mathrm{Ma}. \tag{36}$$

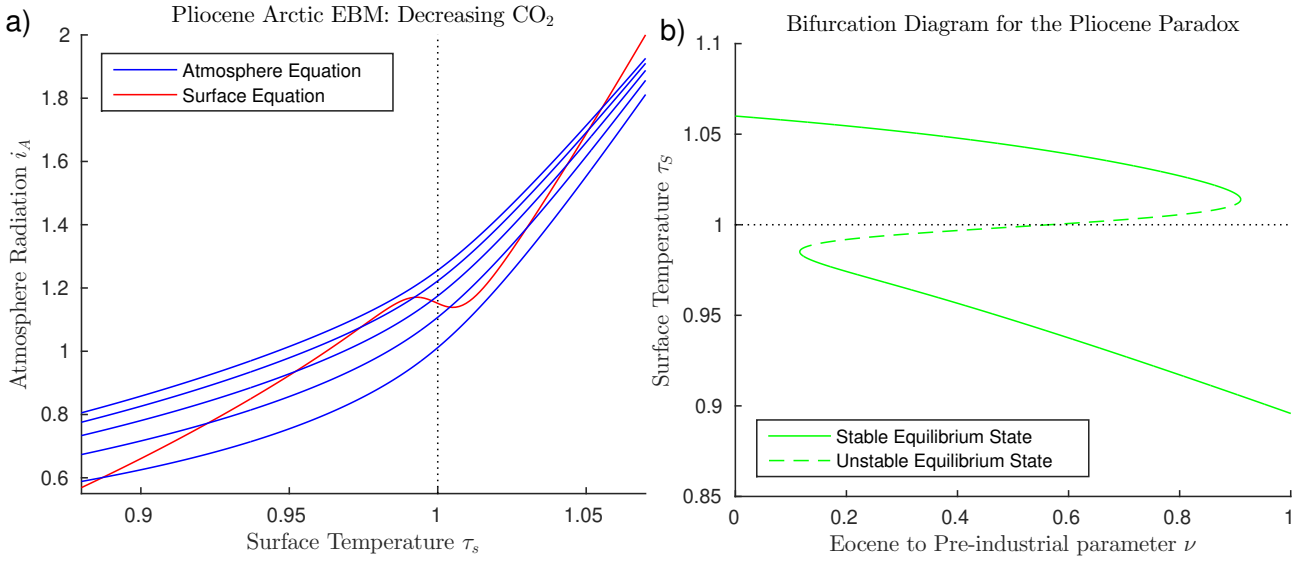

Figure 4. Pliocene Arctic EBM (9)–(10). Parameter values $\delta = 0.67$, ~~$F_A = 115$; other parameters as in Table 1~~ $F_A = 45$ Wm^{-2}, $Q = 173.2$ Wm^{-2}, $\alpha_W = 0.08$, $Z = 9$ km. ~~Subfigure~~ a) ~~:~~ CO_2 takes values ~~$\mu = 1200, 1000, 800, 600, 400, 200$~~ $\mu = 200, 500, 800, 1100, 1400$ ppm, from ~~top to~~ bottom to top on the blue curves, with fixed $F_O = 50$ Wm^{-2} on the red curve. The warm equilibrium state $\tau_S > 1$ disappears as μ decreases on successively lower blue curves. ~~Subfigure~~ b) ~~:~~ Bifurcation Diagram for the Pliocene Paradox. Here, CO_2 concentration μ and ocean heat transport F_O decrease simultaneously, with increasing ν, $(0 \le \nu \le 1)$, as given by ~~equations~~ Equations (37). As ν increases, the warm equilibrium solution ($\tau_S > 1$) disappears in a saddlenode bifurcation, at approximately ~~$\nu = 0.9$~~ $\nu = 0.91$, corresponding to forcing ~~parameter $\mu = 343$~~ parameters $\mu = 336$ ppm and ~~$F_O = 51$ Wm^2~~ $F_O = 50.9$. The equilibrium temperatures at this value of ν are 3.9C and -26C, and geological time about 4.5 Ma. To the right of this point, only the frozen equilibrium state exists. ~~To the left of this point~~Between about $\nu = 0.12$ and $\nu = 0.91$, the frozen and warm equilibrium states coexist, separated by the unstable intermediate state.

~~Then~~ As reviewed above, it is believed that ocean heat transport F_O decreased modestly over this time period, mainly due to the drop in global sea level, while the CO_2 concentration μ decreased more significantly. Therefore, we express both μ and F_O as decreasing ~~linear functions of~~ functions of *bifurcation parameter* ν

$$\begin{aligned} \mu &= \quad 1000 - 730 \cdot \nu \quad \text{ppm} \\ F_O &= \quad 60 - 10 \cdot \nu \quad \text{Wm}^{-2}. \end{aligned} \tag{37}$$

Here, $\nu = 0$ corresponds to estimated mid-Eocene values of μ and F_O, (taken from Pagani et al. (2005); Wolfe et al. (2017); Barron et al. (1981)), while $\nu = 1$ corresponds to modern preindustrial values (IPCC (2013)). Equations (37) define μ and F_O as linear functions of ν~~, just as did for the Antarctic model~~. In the real world, neither μ nor F_O decreased linearly. This is not an obstacle for our bifurcation analysis. What is important is that, somewhere between $\nu = 0$ and $\nu = 1$, a bifurcation point is crossed.

Figure 4 ~~b) b~~ is a bifurcation diagram~~(Kuznetsov (2004)), ,~~ which shows the dependence of surface temperature τ_S on this bifurcation parameter ν. Note that, for ~~$\nu = 0$~~ $\nu = 0$ (mid-Eocene values, 50 Ma) ~~both the warm and the~~ only the warm equilibrium state exists. At about $\nu = 0.116$ (44 Ma) both warm and frozen equilibrium states exist. However, as ν increases toward $\nu = 1$, the warm equilibrium state disappears in a saddlenode (or fold) bifurcation, leaving only the frozen equilibrium state to the right of the saddlenode bifurcation. This bifurcation occurs at approximately ~~$\nu = 0.9$, which correspondis to $\mu = 343$ ppm and $F_O = 51$ Wm^{-2}. The~~ $\nu = 0.91$, which corresponds to $F_O = 50.9$ Wm^{-2} and $\mu = 336$, which is in good agreement with the determination of Seki et al. (2010) that the warm Pliocene pCO_2 was between 330 and 400 ppm, similar to today. The temperatures of the warm state and frozen state~~temperatures~~, at the bifurcation value of ~~$\nu = 0.9$~~ $\nu = 0.91$ in the EBM, are ~~$+4.1°$C and $-27.9°$C; reasonably close to actual Pliocene values~~ $+3.9°$C and $-26°$C. The surrogate time of the bifurcation point, ~~$\nu = 0.9$~~$\nu = 0.91$, corresponds to a geological time of ~~$t = 5$~~ $t = 4.5$ Ma, from (36), which is close to the time of glaciation of the Arctic in the geological record.

~~Thus, the EBM presented here, as illustrated~~ The EBM plotted in Figure 4 ~~,~~ provides a plausible explanation for the Pliocene paradox. ~~The~~ For millions of years up to the mid-Pliocene, while the Arctic temperature remained above freezing on the warm solution branch in Figure 4b, the climate change was incremental. Then the slowly-acting physical forcings of decreasing CO_2 concentration and decreasing ocean heat transport F_O were amplified by the mechanisms of ice-albedo feedback and water vapour feedback, both of which act very strongly when the temperature crosses the freezing point of water. ~~For millions of years before the Pliocene, while the Arctic temperature remained well above freezing, the climate changed very little. However, once~~ The EBM suggests that when the freezing temperature was ~~reached~~approached, the Arctic climate changed abruptly via a saddlenode bifurcation as in Figure 4 ~~b), to a new~~ b, from a warm state to a frozen state. ~~This simple mechanism suffices to explain~~

3.1.1 Permanent El Niño

Another explanation has been proposed for the Pliocene paradox. ~~No more complicated explanations are necessary.~~

~~To summarize this section, there are in fact four different "paradoxes" associated with the Arctic climate~~ There is convincing evidence that, at the beginning of the Pliocene~~Epoch. Each of these paradoxes is resolved by the EBM of this paper, as follows.~~

~~The early Pliocene~~Arctic climate was warm and equable, very different from today's climate, even though all of the forcing ~~factors were very similar to those of today. The EBM explains that the climate system under Pliocene forcing conditions possessed two different climate states, a warm state like the early Pliocene climate and a frozen state like today's climate, coexisting mathematically for the same forcings.~~ , there was a permanent El Niño condition in the tropical Pacific ocean, see Fedorov et al. (2006, 2010); Steph et al. (2010); Cronin (2010); von der Heydt and Dijkstra (2011). (However, some have disputed this finding, see Watanabe et al. (2011).) It has been suggested that a permanent El Niño condition could explain the warm early Pliocene, and that the onset of the El Niño – La Niña Southern Oscillation (ENSO) was the cause of sudden cooling of the Arctic during the Pliocene. Today, it is known that ENSO can influence weather patterns as far away as the Arctic. However, the present authors propose that bistability and bifurcation provide a more satisfactory explanation for the

Pliocene paradox, and suggest that the concurrent change in ENSO may have been a consequence, not the cause, of the changing Pliocene Arctic climate (work in progress).

~~In the mid-Pliocene,~~

3.2 EBM for the Glaciation of Antarctica

Antarctica in the mid-Cretaceous Period was ice-free, and it remained so for the remainder of the Cretaceous Period and into the Paleocene and early Eocene. However, recent investigations in paleoclimate science have shown that there was an abrupt drop in temperature and an onset of glaciation in Antarctica, at the Eocene-Oligocene Transition (EOT) about 34 Ma; see Katz et al. (2008); Lear et al. (2008); Miller et al. (2008); Scher et al. (2011, 2015); Ladant et al. (2014); Ruddiman (2014). In the mid-Cretaceous, the continent of Antarctica was in the South Pacific Ocean and the South Pole was located in open ocean, warmed by South Pacific Ocean currents (Cronin (2010)). Then, the ~~Arctic climate underwent a major and rapid excursion, from warm to frozen, even though the forcing factors were changing very slowly at the time. The EBM indicates that the climate state underwent a saddlenode bifurcation at this time, causing an abrupt transition from a warm to a frozen state.~~

~~The planet Earth has a remarkable North-South symmetry, with respect to all external forcing factors that determine the climate. Yet, for about 30 million years prior to the Pliocene, the Antarctic was ice-covered while the Arctic was ice-free. Decreasing carbon dioxide concentration μ caused cooling at both poles; however, μ is the same throughout the atmosphere at any given time. The EBM identifies ocean heat transport F_O as the forcing factor responsible for breaking the North-South symmetry of the planet. Due to the movement of the continental tectonic plates, ocean currents have changed significantly in the past 100 million years. For the South Pole, the effect was to reduce F_O from a very high valueto a very low value; while for the North Pole, the net reduction in F_O was quite small. This more rapid cooling of Antarctica caused glaciation to occur there~~ continent of Antarctica moved poleward and began to encroach upon the South Pole towards the end of the Cretaceous, fully covering the South Pole before the end of the Eocene (Briggs (1987)). The diminishing marine influence on the South Pole coincided with the onset of cooling of Antarctica about 45 Ma (mid-Eocene). The opening of both the Drake Passage (between South America and Antarctica) and of the Tasmanian Gateway (between Antarctica and Australia) near the end of the Eocene (34 Ma), led to the development of the Antarctic Circumpolar Current (ACC), which further isolated the South Pole from warm ocean heat transport and accelerated the cooling and glaciation of Antarctica; Cronin (2010). Therefore, from the early Eocene to the Oligocene, the ocean heat transport to the South Polar region decreased significantly, from near the Cretaceous value, about 100 Wm^{-2} (Barron et al. (1981)), to a much lower value, estimated here to be 30 Wm^{-2}. The fact that the glaciation of the Antarctic took place 30 million years before the glaciation of the Arctic very likely is due primarily to the much larger decrease in ocean heat transport that took place at the South Pole.

~~General Circulation models (GCM), which accurately reproduce today's climate, fail to duplicate the early Pliocene warm climate when adjusted to early Pliocene forcings. The EBM suggests that these GCM simulations, starting with today's climate and moving backward in time, would have remained on the stable frozen climate state of the bifurcation diagram in Figure 4 b), and thus failed to "see" the coexisting warm state.~~ Because the atmosphere is well mixed, at any given time the CO_2 level in the Antarctic is the same as elsewhere. For this EBM, we estimate early Eocene global CO_2 level as $\mu = 1100$ ppm,

(Pagani et al. (2005, 2006); Cronin (2010)); decreasing to approximately modern levels by the end of the Oligocene, 23 Ma, that is to $\mu = 400$ ppm.

In the recent literature, there has been a discussion of whether the primary cause of the onset of Antarctic glaciation is the slow decline in CO_2 concentration, or the decrease in poleward ocean heat transport due to the opening of ocean gateways and the development of the ACC; see DeConto et al. (2008); Goldner, et al. (2014); Pagani et al. (2011); Scher et al. (2015). In fact, Ladant et al. (2014) state "The reasons for this greenhouse-icehouse transition have long been debated, mainly between the tectonic- oceanic hypothesis and the CO2 hypothesis". In the work of Scher et al. (2015), it is observed that onset of the ACC coincided with major changes in global ocean circulation, which probably contributed to the drawdown in CO_2 concentration in the atmosphere. Since both CO_2 concentration and ocean heat transport F_O are explicit parameters in the EBM presented here, they can be varied independently in the model to investigate which one played a primary role.

3.2.1 ~~Permanent El Niño and Hadley cell feedback~~

~~Several other explanations have been proposed for the Pliocene paradox. There is convincing evidence that, at the beginning of the Pliocene, there was a permanent El Niño condition in the tropical Pacific ocean, see Cronin (2010); Fedorov et al. (2006, 2010) . (However, some have disputed this finding, see Watanabe et al. (2011).) It has been suggested that a permanent El Niño condition could explain the warm early Pliocene, and that the onset of the El Niño – La Niña Southern Oscillation (ENSO) was the cause of sudden cooling of the Arctic during the Pliocene. Today~~ Figure 5 shows the solutions of the EBM equations for Antarctic parameter values, including $\delta = 0.67$, $F_A = 45$ Wm^{-2}, $Q = 173.2$ Wm^{-2}, $\alpha_W = 0.15$, and $Z = 9$ km. Points of intersection of one red line (surface equation) and one blue line (atmosphere equation) are the equilibrium solutions of the system. As noted earlier, there can be up to three equilibrium solutions. In Figure 5a the ocean heat transport F_O is held fixed, while CO_2 concentration μ is decreased, from the top to bottom blue lines. In Figure 5b the reverse is true; the CO_2 concentration μ is held fixed while the ocean heat transport F_O is decreased, from bottom to top red lines. For a sufficiently small value of F_O, the warm solution disappears in Figure 5b. This occurs when the warm solution meets the unstable intermediate solution in a saddlenode bifurcation. Beyond this bifurcation, only the frozen solution ($\tau_S < 1$) exists. In contrast, reducing μ in Figure 5a does not affect the existence of the warm equilibrium, only the existence of the cold equilibrium.

Figure 6 displays bifurcation diagrams, in which the surface temperature τ_S, which has been determined as a solution of the EBM, is plotted while parameters in the EBM are varied smoothly, from the early Eocene values, 55 million years ago, to the late Oligocene values, 23 million years ago. These dates are chosen to bracket the time of the glaciation of Antarctica. First we introduce a *bifurcation parameter* ν, which acts as a surrogate time variable. The bifurcation parameter ν is related to geological time by

$$t = 55 - 32 \cdot \nu \quad \text{Ma.} \tag{38}$$

Thus, $\nu = 0$ corresponds to the early Eocene 55 Ma and $\nu = 1$ corresponds to the late Oligocene 23 Ma. During this time, it is known that ~~ENSO can influence weather patterns as far away as~~ both CO_2 concentration μ and ocean heat transport F_O were

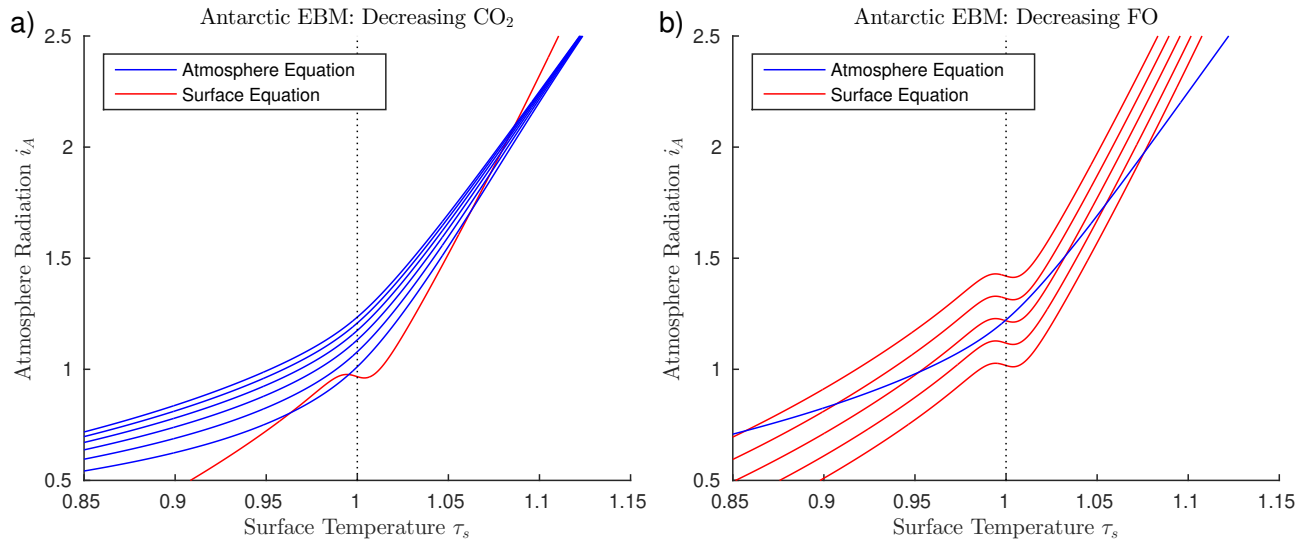

Figure 5. EBM for the Glaciation of Antarctica (with $\delta = 0.67$, $F_A = 45\ \mathrm{Wm}^{-2}$, $Q = 173.2\ \mathrm{Wm}^{-2}$, $\alpha_W = 0.15$, $Z = 9$ km). a) Graphs of EBM equations, with F_O fixed at 90 Wm^{-2} in the surface equation (red line), and with CO_2 concentration μ in the atmosphere equation increasing (from bottom to top blue lines) $\mu = 200, 400, 600, 800, 1000, 1200$ ppm. b) Graphs of the same EBM equations, but with CO_2 concentration μ fixed at 1100 ppm (blue line) and with ocean heat transport F_O decreasing (from bottom to top red lines) 80, 60, 40, 20, 0 Wm^{-2}.

decreasing. To study the effects of the simultaneous reduction of μ and F_O, we express both as simple linear functions of the bifurcation parameter ν, as follows:

$$\begin{aligned} \mu &= 1100 - 700 \cdot \nu, \\ F_O &= 100 - 70 \cdot \nu, \qquad 0 \le \nu \le 1. \end{aligned} \tag{39}$$

Here, $\nu = 0$ corresponds to the high early Eocene values of $\mu = 1100$ ppm and $F_O = 100\ \mathrm{Wm}^{-2}$, while $\nu = 1$ corresponds to the low Oligocene-Miocene boundary values of $\mu = 400$ ppm and $F_O = 30\ \mathrm{Wm}^{-2}$. Thus, in Equations (39), as ν increases from 0 to 1, the climate forcing factors μ and F_O decrease linearly from their Eocene values to late Oligocene values. Strictly speaking, these forcings did not change linearly in time; however, the important fact is that overall they were decreasing. For our bifurcation results the decrease does not need to be linear in the EBM. The atmospheric heat transport parameter F_A is held constant at $F_A = 45\ \mathrm{Wm}^{-2}$. The solar radiation is $Q = 173.2\ \mathrm{Wm}^{-2}$, the warm albedo value is $\alpha_W = 0.15$, and the tropopause height is $Z = 9$ km. Other parameters are as in Table 1.

Figure 6a shows a saddlenode bifurcation at $\nu = 0.779$, corresponding to forcing parameter values $\mu = 555$ ppm and $F_O = 45.5\ \mathrm{Wm}^{-2}$ in the ~~Arctic~~ model, and to geological time about 30 Ma, assuming the linear time relation in (38). This corresponds closely to best estimates of the timing of glaciation in the geological record of about 34 Ma at the EOT. This quantitative agreement should not be taken very seriously, as it is largely due to assumptions made in the modelling.

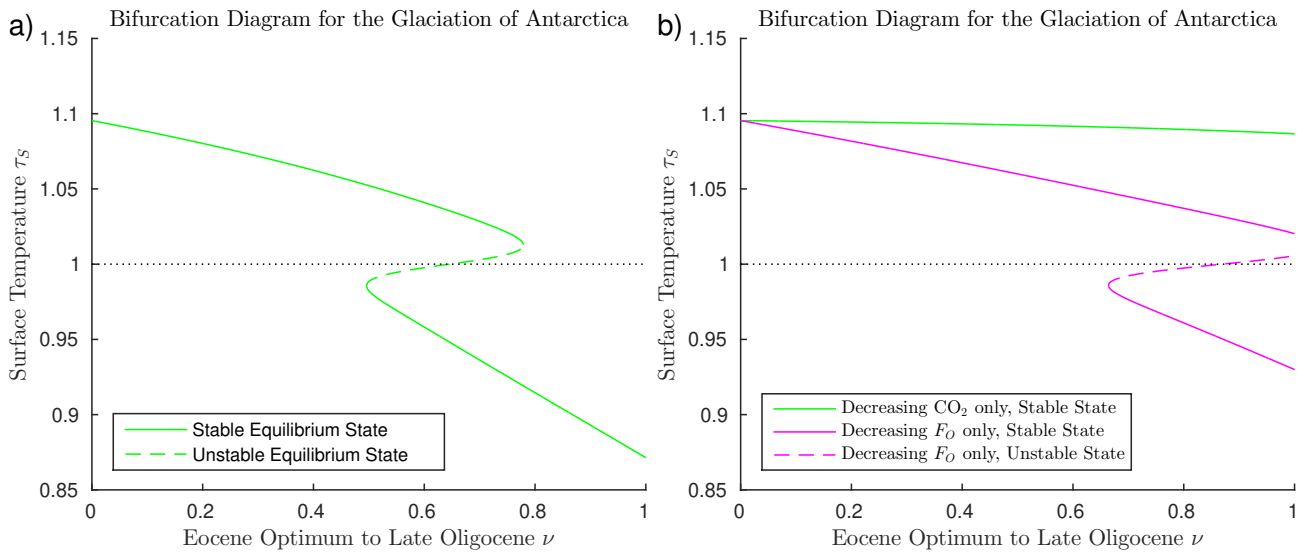

Figure 6. Bifurcation Diagrams for the Glaciation of Antarctica (with $\delta = 0.67$, $F_A = 45\ \mathrm{Wm}^{-2}$, $Q = 173.2\ \mathrm{Wm}^{-2}$, $\alpha_W = 0.15$, $Z = 9$ km). a) This shows a saddlenode bifurcation at $\nu = 0.779$, corresponding to forcing parameter values $\mu = 555$ ppm and $F_O = 45.5\ \mathrm{Wm}^{-2}$ in Equations (39). As ν increases through this saddlenode bifurcation point, the climate will transition abruptly from a warm state to a frozen state. The warm state and frozen state temperatures coexisting at the bifurcation point are $+3.5°\mathrm{C}$ and $-22.1°\mathrm{C}$. b) Two superimposed bifurcation diagrams as in a), except that, on the green curve, F_O is held fixed at its Eocene values while μ deceases as in (39), and on the magenta curve, μ is held fixed at the Eocene value while F_O decreases as in (39). No saddlenode bifurcation destroying the warm equilibrium occurs in either scenario.

However, the *existence* of the bifurcation, implying an abrupt glaciation of Antarctica, can be taken seriously, as this is a robust (structurally stable) property of the model. The warm state and frozen state temperatures coexisting at the bifurcation point are $+3.5°\mathrm{C}$ and $-22.1°\mathrm{C}$. As ν increases past the bifurcation point $\nu = 0.779$, the warm climate state ceases to exist, and the climate system transitions ("falls") rapidly, from the saddlenode point to the frozen state. Thus the EBM reproduces the abrupt transition to the glaciation of Antarctica, which is seen in the geological record at the EOT.

~~Another suggestion is that Hadley cell feedback contributed to~~ Figure 6b explores the relative importance of decreasing CO_2 concentration μ and decreasing ocean heat transport F_O in the ~~abrupt cooling of the Arctic during the Pliocene. Recent work shows that an increase in pole-to-equator temperature gradient causes the Hadley cells to contract towards the equator, while increasing in circulation velocity, see Lewis and Langford (2008); Langford and Lewis (2009). This would cause a decrease in equator to pole atmospheric heat transport, which would in turn accelerate Arctic cooling; this is called Hadley cell feedback. Further work on modelling this mechanism is in progress. It is conjectured here that Hadley cell feedback may in fact have caused the end of a permanent El Niño condition in the Pliocene, as follows. It is known that the La Niña phase of ENSO is forced in part by the Trade Winds blowing East to West across the tropical Pacific Ocean. The Trade Winds are the surface component of~~ glaciation of Antarctica, a subject that has been much debated in the literature (DeConto et al. (2008); Goldner, et al. (2014);

Forcing Parameter Values for the Tropics EBM		
Parameter	**Modern Arctic Value**	**Tropics Value**
Relative humidity δ	~~0.4~~ 0.67	~~0.7~~ 0.85
Ocean heat transport F_O	~~20-60~~ 20–60 Wm^{-2}	~~-20~~ -50 Wm^{-2}
Atmospheric heat transport F_A	~~70-120~~ 45 Wm^{-2}	~~-18~~ -25 Wm^{-2}
~~Latent heat transport F_C 0 Wm^{-2} 80 Wm^{-2}~~ Warm surface albedo α_W	0.08	~~0.04 Frozen surface albedo α_C 0.7 0.7~~ 0.08
Incident solar radiation Q	173.2 Wm^2	418.8 Wm^{-2}
Tropopause height Z	9 km	17 km

Table 2. Summary of parameters used in the Tropics EBM. Relative humidity δ is higher in the Tropics that the Arctic, and the forcings F_O and F_A are negative instead of positive. The ~~forcing F_C is explained in the text. The~~ insolation Q is as determined by McGeehee and Lehman (2012). Tropopause height Z is from Kishore et al. (2006). Parameters not listed here are ~~the same~~ as ~~for the Arctic, see~~ in Table 1.

), The green curve represents a scenario in which μ decreases as in Equation (39) but F_O is held fixed at its Eocene value, and the magenta curve represents a case in which μ is held fixed at its Eocene value while F_O decreases according to (39). In neither case does a glaciation event occur. The analysis of this paper implies that significant decreases in *both* CO_2 concentration μ *and* ocean heat transport F_O are required to achieve a saddlenode bifurcation, reproducing the observed transition to a frozen Antarctic state at the EOT.

While the glaciation of Antarctica is an accepted fact in paleoclimate science (Miller et al. (2008); Lear et al. (2008); Pagani et al. (2011)) the suddenness of the climate change that occurred in Antarctica near the Eocene-Oligocene Transition (34 Ma), a time when the forcing parameters were changing slowly, has been difficult to explain. The bifurcation analysis presented here presents a simple but plausible explanation for the ~~Hadley circulation. Therefore, acceleration of the Hadley circulation would strengthen the Trade Winds, enhancing the conditions for La Niña and ending the permanent El Niño. Further work on this conjecture also is in progress~~abruptness of this event. Furthermore, this EBM supports the hypothesis that both falling CO_2 concentration μ and decreasing ocean heat transport F_O (due to gateway openings and development of the ACC) are essential to an explanation of the sudden glaciation of Antarctica at the EOT.

3.3 EBM for the Tropics

In the Tropics, many of the values of the forcing parameters are different from their values in the Arctic and Antarctic, see Table 2. The geological record shows little change in the tropical climate over the past 100 million years, other than ~~a little~~ minor cooling. Even when the Arctic climate changed dramatically in the Pliocene, the Tropical climate changed very little.

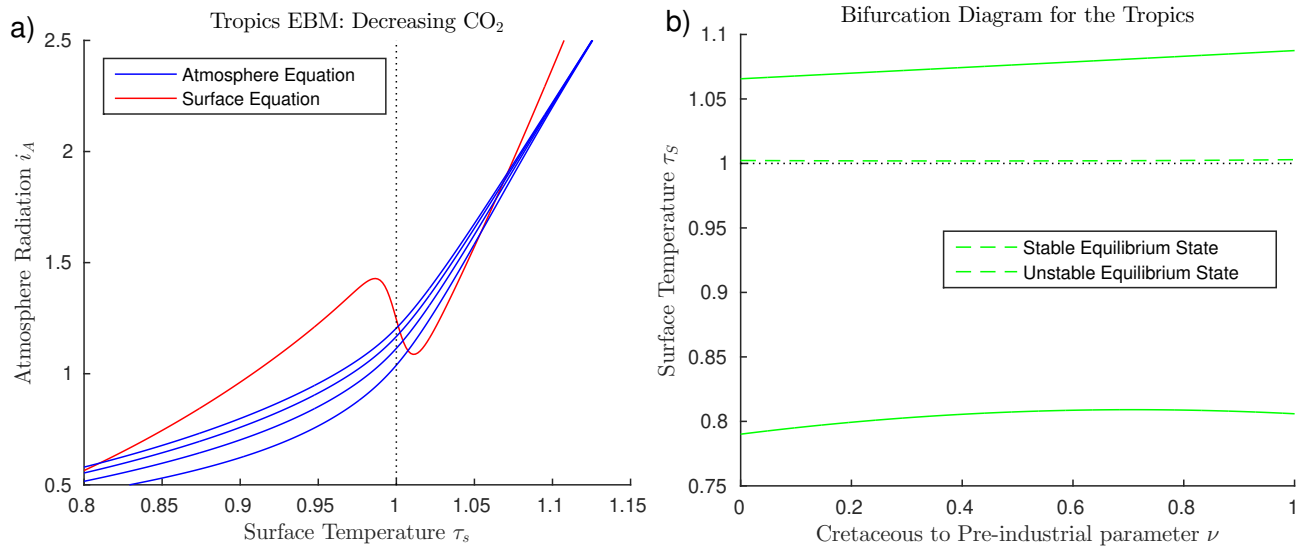

Figure 7. Tropics EBM, using ~~equations~~ Equations (9)~~–~~(10) and parameter values as in Table 2. ~~Subfigure~~ a) ~~:~~ The blue curves represent the atmosphere equilibrium equation for ~~$\mu = 1200, 900, 600, 300$~~ $\mu = 300, 600, 900, 1200$, from ~~top to~~ bottom to top. ~~Subfigure~~ b) ~~:~~ Bifurcation Diagram for the Tropics EBM. Here, CO_2 concentration μ and ocean heat transport F_O are both decreasing, with increasing ν, $(0 \leq \nu \leq 1)$, as given by ~~equations~~ Equations (40). As ν varies, both the warm equilibrium state ($\tau_S > 1$) and the frozen equilibrium state ($\tau_S < 1$) persist; there are no saddlenode bifurcations.

~~The new entry in this Table, one that did not appear in the polar models, is F_C, which represents transport of heat away from the surface to the atmosphere, by conduction / convection / change of state of water. The most important of these is the upward transport of latent heat. Surface water evaporates, taking heat from the surface. As warm moist air rises and cools, the water vapour condenses, releasing its latent heat into the surrounding atmosphere. This transfer is estimated at about $F_C = 80\ \mathrm{Wm}^{-2}$ in the Tropics (IPCC (2013)). In the surface energy balance equation this quantity is negative, while in the Atmosphere equation its contribution is positive. After normalization, $f_C = \frac{F_C}{\sigma T_R^4}$. With these changes, the EBM becomes, for the Tropics~~

$$i_A \equiv f_A + f_C + \eta_{CW}(\tau_S) \cdot \tau_S^4,$$

$$i_A \equiv \frac{1}{\beta}\left(\tau_S^4 - [1 - \alpha(\tau_S)]\, q + f_C - f_O\right).$$

Figure 7a ~~)~~ shows solutions of ~~these~~ the EBM equations for Tropical parameter values. Note that at no value of the forcings used here does the warm equilibrium point approach a saddlenode bifurcation point. Thus, our EBM is in agreement with the geological record.

A bifurcation diagram is constructed for the Tropics EBM, spanning mid-Cretaceous to modern pre-industrial times, similar to those for the Antarctic and Arctic glaciations. Here $\nu = 0$ corresponds to mid-Cretaceous values and $\nu = 1$ corresponds to

modern pre-industrial values. We let μ and F_O decrease linearly with ν.

$$\begin{aligned} \mu &= 1130 - 860 \cdot \nu \\ F_O &= -55 + 29 \cdot \nu. \end{aligned}$$

$$\begin{aligned} \mu &= 1130 - 860 \cdot \nu, \\ F_O &= -55 + 29 \cdot \nu, \qquad 0 \le \nu \le 1. \end{aligned} \tag{40}$$

The mid-Cretaceous CO_2 concentration $\mu = 1130$ ppm is as determined by Fletcher et al. (2008), see Table 3. The ocean heat transport ~~$F_O = -55$~~$F_O = -55$ Wm^{-2}, from the Tropics in the mid-Cretaceous, is from Barron et al. (1981). Astrophysicists have determined that solar luminosity is slowly increasing with time (Sagan and Mullen (1972)). For the mid-Cretaceous, insolation was approximately 1% less than it is today (Barron (1983)). This difference is considered too small to be significant in our model. The bifurcation diagram for the Tropics EBM is shown in Figure 7 ~~b)~~b. Note that no bifurcations occur for parameter values relevant to the Tropics. This is in agreement with paleoclimate records that show little change in Tropical climate, even when polar climates ~~change~~ changed dramatically.

3.4 EBM for the Cretaceous and Eocene Warm Equable ~~Cretaceous Problem~~Climate Problems

One hundred million years ago, in the mid-Cretaceous period, the climate of Earth was much more *equable* than today. "More equable" means that the pole-to-equator temperature gradient was much smaller, and also the seasonal summer/winter temperature variations were much smaller. The climate in the Tropics was only slightly warmer than today, but the climate at both poles was much warmer than today. An abundance of plant and animal life thrived under these conditions, from the equator to both poles, including of course dinosaurs. The question of how this globally ice-free climate could have been maintained ~~has been called a fundamental problem in paleoclimatology (Barron et al. (1981); Barron (1983); Cronin (2010)).~~

~~There have been many attempts to explain this difference in climate (Bice et al. (2006); Barron et al. (1981, 1995); Barron (1983); Cronin).~~ was explored in pioneering work of Barron and coworkers (Barron (1983); Barron et al. (1981, 1995); Sloan and Barron (1992)). Barron called this the *warm, equable Cretaceous climate problem*. Early General Circulation Models (GCM) of the 1980's, adjusted to mid-Cretaceous forcing parameter values~~have failed to give~~ , had difficulty giving good agreement with climate proxies. In order to obtain polar temperatures in agreement with mid-Cretaceous values, these simulations typically ~~have~~ assumed increased CO_2 levels more than 4 times modern levels; but then the tropical temperatures predicted by the models were too high. ~~Barron (1983) called this the *warm, equable Cretaceous climate problem*. Later, Sloan and Barron (1990) speculated that continental interiors had cold winters even in the Cretaceous; however, that proposal has been challenged (Wing and Greenwood (1993)~~

There have been many investigations of the correlation between early climate models and proxy data for the Cretaceous climate (Pagani et al. (2005); Bice et al. (2006); Donnadieu et al. (2006); Cronin (2010); Ruddiman (2014)). Recent studies have succeeded in narrowing the gap (Craggs et al. (2012); Bowman et al. (2014); O'Brien et al. (2017); Lunt et al. (2016); Ladant and Donnadi

). Based on ocean drilling samples, Bice et al. (2006) estimate Cretaceous CO_2 concentrations between 600 ppmv and 2400 ppmv, and tropical Atlantic upper ocean temperatures between 33°C and 42°C. Based on fossil samples, Fletcher et al. (2008) estimate mid-Cretaceous atmospheric CO_2 concentrations of 1130 ppmv and we choose their estimate for use in this EBM, see Table 3.

Forcing Parameters for the mid-Cretaceous EBM, 100 Ma			
Parameter	~~mid-Cretaceous~~ **Arctic Value**	**Antarctic Value**	**Source**
CO_2 level μ	1130 ppm	1130 ppm	Fletcher et al. (2008)
Relative humidity δ	0.67	0.67	Jahren and Sternberg (2003)
~~Antarctic ocean heat transport~~ Ocean heat transport F_O	~~100~~ 22 W m^{-2}	~~Barron et al. (1981) Arctic ocean heat transport F_O 60~~ W m^{-2}	Barron et al. (1981)
Atmospheric heat transport F_A	~~41~~ 56 W m^{-2}	25 W m^{-2}	Barron et al. (1981)

Table 3. Summary of parameters used in the Polar ~~Cretaceous~~ mid-Cretaceous model. The main difference in Cretaceous climate between the two poles was that ocean heat transport was much higher in the Antarctic. Parameters not listed here are the same as ~~for today's Arctic, see~~ in Table 1. The ~~value~~ values of F_A and F_O shown here ~~is an average of estimates in~~ are estimated from Barron et al. (1981).

~~Solutions of the mid-Cretaceous EBM for both poles, using parameter values in Table 3. The blue curve represents the atmosphere equilibrium equation, which is the same for both poles. The two Z-shaped curves represent the Arctic (upper orange curve) and the Antarctic (lower magenta curve) surface equilibrium equations. The only difference in these two is that ocean heat transport F_O is much greater in the Antarctic than the Arctic. Both poles support both warm and frozen equilibrium states. (This figure is referenced also in Section ??.)~~

Paleoclimate data from the mid-Cretaceous show little difference in climate between the two warm poles at that time ~~.~~ ~~However, major changes in climate have taken place since that time, at both poles.~~ (Barron et al. (1981); Barron (1983)). The major difference in forcings between the two poles at that time was that ocean heat transport F_O was much higher in the Antarctic than the Arctic, as shown in Table 3. This is due to the location of the South Pole in open ocean during the Cretaceous, as the continent of Antarctica had not yet drifted to its present position over the South Pole. Estimates for atmospheric transport are also different Barron et al. (1981). Therefore, we model the mid-Cretaceous climate at the two poles using ~~equations , with two values of F_O as in~~ Equations (9)–(10), with the values from Table 3~~, and all other forcings the same for the Arctic and Antarctic.~~

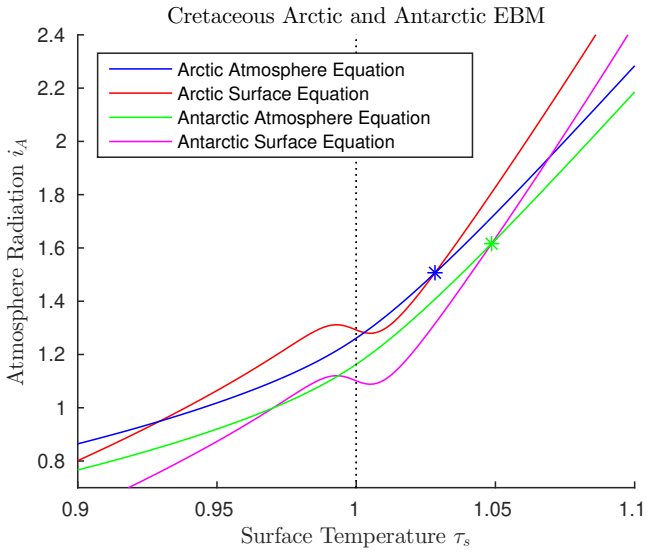

Figure 8. Solutions of the mid-Cretaceous EBM for both poles, using parameter values in Table 3. The blue and orange curves represent the EBM for the Arctic while the green and magenta curves represent the Antarctic. The two Z-shaped curves represent the surface equilibrium equations for the Arctic (upper orange curve) and the Antarctic (lower magenta curve) . The only differences in these two is that ocean heat transport F_O is much greater in the Antarctic than the Arctic, and the atmospheric transport, F_A, is smaller. Both poles support both warm and frozen equilibrium paleoclimate states. The warm equilibrium states at the two poles are marked by stars.

. The EBM equilibrium curves are shown in Figure 8, where it is clear that a warm ($\tau_S > 0$) and a frozen ($\tau_S < 0$) equilibrium state exists at both poles, for the given parameter values. The Antarctic warm equilibrium state is ~~the warmer of the two~~warmer than in the Arctic, because of the higher ocean heat transport F_O to the Antarctic. From Section 3.3, the Tropical region of Earth also had a warm equilibrium state under mid-Cretaceous conditions. Therefore, the EBM of this paper implies existence of a pole-to-pole, warm, equable Cretaceous climate, as is seen in the geological record.

Figure 8 also implies that a frozen equilibrium state is mathematically possible at each pole during the Cretaceous. In that case, the Tropics could remain in ~~its~~ the warm state, thus giving the mathematical possibility of a Cretaceous climate that is *not equable*, but has warm Tropics and ice-covered poles, like today's climate. This may help explain why some computer simulations, ~~starting from~~ originally designed for today's climate conditions, found a mathematically existing Cretaceous climate that resembled today's climate, rather than the warm, equable climate that ~~actually existed~~ physically existed on Earth in the Cretaceous.

3.5 ~~EBM for the Eocene Equable Climate Problem~~

The climate of the ~~early~~ Eocene Epoch (~~≈ 50~~ ≈ 55 million years ago) was the warmest of the past 65 million years, but a little cooler than the Cretaceous, see ~~Cronin (2010); Pagani et al. (2005); Sloan and Barron (1992); Sloan and Rea (1995)~~

Sloan and Barron (1992); Pagani et al. (2005); Cronin (2010); Huber and Caballero (2011); Hutchinson et al. (2018). Both poles were ice-free and the pole to equator temperature gradient was much smaller than today. ~~Computer~~ As for the mid-Cretaceous, early computer simulations, based on modern climate conditions, ~~have failed to reproduce~~ had difficulty in reproducing the early Eocene warm equable climate, see ~~Huber and Caballero (2011); Jahren and Sternberg (2003); Sloan and Barron (1990, 1992)~~ Sloan and Barron (1990, 1992); Sloan and Rea (1995); Jahren and Sternberg (2003); Huber and Caballero (2011). This discrepancy has been called the *early Eocene warm equable climate problem*. Here we combine these two "problems" under the name of the *warm equable Paleoclimate problem*.

The main difference in forcings between early Eocene conditions and those of the mid-Cretaceous, is that the global CO_2 concentration μ may have been a little lower and the ocean heat transport F_O to the Antarctic was less. Referring to Figure 8, this means that the blue ~~atmosphere equilibrium curve moves downward slightly~~and green atmosphere equilibrium curves move downward slightly, and the magenta Antarctic surface equilibrium curve moves upward slightly. The orange Arctic surface equilibrium curve does not change significantly. With these small changes, all of the equilibrium climate states (intersection points) persist in Figure 8. ~~Therefore, adaptation of the EBM of this paper to early Eocene climate conditions yields results very similar to those of Section 3.4 for the mid-Cretaceous climate.~~ The figure for the Eocene EBM (not shown here) is topologically the same as Figure 8 for the mid-Cretaceous EBM,

Thus, the EBM predicts that a warm~~(~~, ice-free ~~)~~ equilibrium state exists (mathematically) at both poles in the mid-Cretaceous and early Eocene. From Section 3.3, the equatorial region also has a warm equilibrium state for Eocene conditions. Therefore, this EBM study supports the existence of a pole-to-pole, warm ~~,~~equable climate in ~~the Eocene Epoch~~both the mid-Cretaceous and the early Eocene. Additionally, in the EBM there is co-existence of a non-equable climate, with cold poles, under exactly the same forcing conditions, which suggests the following plausible solution to the "warm equable paleoclimate problem" in both the mid-Cretaceous [Barron et al. (1981); Barron (1983); Sloan and Barron (1990); Barron et al. (1995)] and the early Eocene [Sloan and Barron (1990, 1992); Sloan and Rea (1995); Jahren and Sternberg (2003); Huber and Caballero (2011)]. While the Earth's climate existed in the warm equable climate state of the EBM, computer simulations of Barron and others may have correctly computed the co-existing non-equable solution.

4 Conclusions and Future Work

This paper presents a new energy balance model (EBM) for the climate of Earth, one that elucidates the distinctive roles of carbon dioxide and water vapour as greenhouse gases, and also the role of ice-albedo feedback, in climate change. Nonlinearity of the EBM leads to multiple solutions of the mathematical equations and to bifurcations that represent transitions between coexisting stable equilibrium states. This EBM sheds new light on several important problems of paleoclimate science; namely, the Pliocene Paradox, the abrupt glaciation of Antarctica, ~~the Pliocene Paradox,~~ and the warm equable mid-Cretaceous ~~climate problem and the warm equable~~ and early Eocene climate ~~problem~~problems. Predictions of the EBM are in qualitative agreement with the paleoclimate record.

~~Some readers may challenge the choices of paleoclimate parameter values used in this paper.~~ There has been a ~~wide~~ range of values ~~published in the paleoclimate~~ of paleoclimate forcing parameters in the literature, in particular for mid-Cretaceous and Eocene CO_2 concentrations and temperatures. The specific choices made here, while informed by proxies, are somewhat arbitrary. However, this fact does not affect the validity of our main conclusions. The *coexistence of multiple solutions* and the *bifurcations* demonstrated in the EBM, are robust phenomena. That is, the existence of these multiple solutions and bifurcations will persist, over a range of values of the forcing parameters. The main conclusion of this paper, that sudden and significant changes in climate have occurred, even while forcing parameters were changing very gradually, follows from the existence of mathematical bifurcations in the EBM, not from particular choices of the forcing parameters.

As the paleoclimate record becomes clearer, there is growing evidence for ~~relatively~~ small but rapid fluctuations in some parameter values, including CO_2 concentrations, over the geological time period studied here; see Cronin (2010); Pagani et al. (1999, 2005). The model of this paper assumes a smooth decline in CO_2 concentration. However, this does not invalidate our main conclusions. The theory of Stochastic Bifurcation (Namachchivaya (1990); Arnold et al. (1996)) tells us that, if stochastic noise is added parametrically to a deterministic bifurcation problem, then typically the location of the bifurcation (in terms of the bifurcation parameter) may change, but the *existence* of the bifurcation is preserved.

Further work on this EBM is in progress. Having demonstrated the ~~validity~~ applicability of the EBM ~~on~~ to known paleoclimate transitions, this EBM is now being applied to anthropogenic climate change, with the goal of predicting the climate effects of continued increases in CO_2 concentration, now and in future centuries. ~~Next, this~~ The Equilibrium Climate Sensitivity (ECS) of the EBM, adapted to present-day satellite data, is presented in Appendix B of this paper.

This scalar EBM will be generalized to a two-point boundary value problem in the altitude variable z, using the Schwarzschild equations to replace the ICAO International Standard Atmosphere approximation for lapse rate. That change will ~~more accurately model~~ model more accurately the behaviour of the greenhouse gases in the atmosphere. Next, ~~the~~ that one-dimensional EBM BVP will be incorporated into a generalization of the spherical shell PDE model of Lewis and Langford (2008); Langford and Lewis (2009). ~~This zonally symmetric~~ We anticipate that this 3D zonally-symmetric Navier-Stokes Boussinesq ~~system~~ model will confirm the fundamental predictions, relating to bistability and bifurcation, of the present simple EBM. Also, it will enable the study of a third positive feedback mechanism (in addition to the two studied in this paper); namely, Hadley cell convection feedback, which influences atmospheric heat transport F_A. ~~Hadley cell feedback appears to have played a role in the warm equable Cretaceous climateproblem,~~

Appendix A: Empirical Calibration of EBM Parameters

Some of the parameters used in the EBM have standard values, available in textbooks and reported in Table 1. Others, however, are determined empirically in this Appendix. Modern values of these parameters may be determined from today's abundant satellite and land-based data. It is assumed that the values determined here remain valid for paleoclimates.

The primary source for these empirical calibrations are the data presented by (Wild et al., 2013, Figure 4) and (Trenberth et al., 2009, Fig . The data from these authors are globally averaged values. We are applying our model to specific regions (the arctic, antarctic,

or tropics) and therefore adjust some of these values as discussed below. We also employ our model with the globally averaged values to give an Equilibrium Climate Sensitivity calculation in Appendix B.

A1 Solar Radiation

The value of the annually averaged solar radiation at either Pole is $Q = 173.2\ \mathrm{Wm}^{-2}$ and at the Equator is $418.8\ \mathrm{Wm}^{-2}$ (McGeehee and Lehman (2012); Kaper and Engler (2013)). Values from Figure 4 of Wild et al. (2013) indicate the globally averaged solar radiation is $Q = 340\ \mathrm{Wm}^{-2}$. Of this, $79\ \mathrm{Wm}^{-2}$ is directly absorbed by the atmosphere, and $76\ \mathrm{Wm}^{-2}$ is reflected by the atmosphere back into space (both primarily due to clouds). Hence we define the two solar radiation fractions

$$\xi_A = \frac{79}{340} = 0.2324 \qquad \text{and} \qquad \xi_R = \frac{76}{340} = 0.2235. \tag{A1}$$

Since we incorporate no information on varying cloud cover in the model, and since there is very little such information for paleoclimates, we assume these values are constant around the globe. Clearly cloud cover is correlated with surface temperature. We also tried making ξ_A and ξ_R vary with T_S in a manner similar to how we model heat conduction/convection, F_C, below, but found no qualitative differences in the results. For this reason, and to keep the model simple, we have kept these values of ξ_A and ξ_R as global constants in our model.

A2 Surface Albedo

The earth's albedo, α, varies considerably depending on the surface features. Typical values are $0.6 - -0.9$ for snow, $0.4 - -0.7$ for ice, 0.2 for crop land and 0.1 or less for open ocean. In previous papers, including Dortmans et al. (2017), the polar albedo α is assumed to jump between two discrete values, a cold albedo α_C for the ice/snow covered surface, when below the freezing temperature, and a warm albedo α_W corresponding to land or open ocean above the freezing temperature; that is,

$$\alpha = \begin{cases} \alpha_c & \text{if } T_S \le T_R, \\ \alpha_w & \text{if } T_S > T_R. \end{cases} \tag{A2}$$

This discontinuous albedo function is conceptually simple but it is not an accurate representation of what would actually happen if the polar region cooled from ice-free to ice-covered. Recall that this model represents the annually averaged climate. As the polar region cools, there will be a transition period in which warm ice-free summers get shorter and cold ice-covered winters get longer. The annually averaged albedo, therefore, would not jump abruptly from low to high constant values as in (A2); it would transition more smoothly between the summer and winter extreme values. Therefore, in this paper we introduce a more realistic (and smooth) sigmoidal albedo given by the hyperbolic tangent function, Equation (5), and reproduced here:

$$\alpha = \frac{1}{2}\left([\alpha_W + \alpha_C] + [\alpha_W - \alpha_C] \tanh\left(\frac{T_S - T_R}{\Omega} \right) \right). \tag{A3}$$

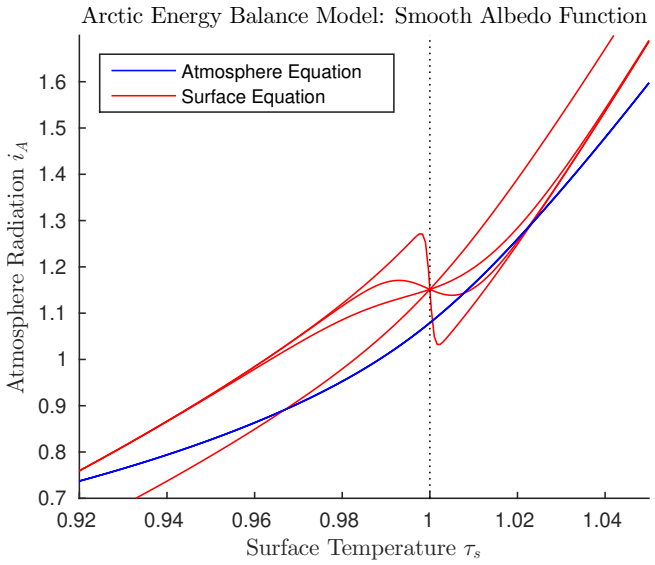

Figure A1. Graphs of the non-dimensionalized EBM Equations (9)–(10). The red curves represent the surface EBM Equation (10). The smooth red curves represent $\alpha(T_S)$ as in (A3), with $\omega \equiv \frac{\Omega}{T_R} = 0.001,\ 0.01,\ 0.02,\ 0.5$, on successively flatter red curves. The blue curve represents the atmosphere Equation (9). There are up to 3 intersections of the blue curve (9) with a given red curve (10) in this figure. Other parameters in the EBM are $\alpha_C = 0.7$, $\alpha_W = 0.08$, $\delta = 0.67$, $\mu = 400$, $F_A = 45\ \mathrm{Wm}^{-2}$, $F_O = 50\ \mathrm{Wm}^{-2}$, $Z = 9$ km.

The parameter Ω determines the steepness of the transition between α_C and α_W. We have chosen $\omega \equiv \Omega/T_R = 0.01$. With this choice, the albedo changes by 80% (that is, it goes from 0.1 to 0.9 of the difference between α_C and α_W) over a span of 6 C in annual mean temperature, which is realistic. See Figure A1.

Figure A1 shows the non-dimensional energy balance equations (9) (in blue) and (10) (in red), for a range of values of the parameter $\omega = \Omega/T_R$ in (A3). The blue (atmosphere) curve may have up to three intersections with a red (surface) curve, implying the existence of multiple equilibrium states.

A3 Average Global Surface Temperature

Both Wild et al. (2013) and Trenberth et al. (2009) indicate that the globally averaged amount of infrared radiation being emitted by the surface of the Earth is 398 W m^{-2}. Since the EBM assumes the Earth is a black body, the Stefan-Boltzmann law dictates that the corresponding temperature is

$$T_S^{\mathrm{avg}} = \left(\frac{398}{\sigma}\right)^{1/4} = 289.45\ \mathrm{K}. \tag{A4}$$

This temperature is equivalent to 16.3°C, which is a little higher than the accepted average surface temperature of about 14°C. This is not surprising since the former is obtained by essentially averaging T^4 while the latter is from averaging actual temperatures. We use the above value for T_S^{avg} in the calibrations described below, since it is consistent with the EBM.

A4 Heat Convection/Conduction and Evapotranspiration

Evapotranspiration (ET) is the transport of water from the surface to the atmosphere, in the form of water vapour. It combines the effects of evaporation from the surface and transpiration by plants. Globally, the largest contributor is evaporation from the surface of the oceans and the main determining factor there is the ocean surface temperature. The ET process also transports heat from the surface to the atmosphere, in the form of latent heat. Recently Wang et al. (2010) have shown that global ET has been increasing over the past several decades.

The forcing term F_C in the EBM represents transport of heat away from the surface to the atmosphere, by conduction plus convection plus change of state of water. The most important of these is the upward transport of latent heat. Surface water evaporates, taking heat from the surface. As warm moist air rises and cools, the water vapour condenses, releasing its latent heat into the surrounding atmosphere. According to both Wild et al. (2013) and Trenberth et al. (2009), the magnitude of this forcing is $F_C = 104\ \mathrm{Wm}^{-2}$. However, this is a globally averaged value and, due to strong dependence on temperature, is not likely valid at other than the globally averaged surface temperature T_S^{avg}. Wang et al. (2010) reports that in the past several decades, ET has increased by $0.6\ \mathrm{Wm}^{-2}$ per decade. Extrapolating back 100 years, this would be $6\ \mathrm{Wm}^{-2}$. In the past century the average global surface temperature has risen about $1°\mathrm{C}$. Thus it is reasonable to assume the dependence of F_C on the surface temperature T_S should have a slope near $T_S = T_S^{\mathrm{avg}}$ of about 6. If the dependence of F_C on T_S was simply linear, then, given that $F_C(T_S^{\mathrm{avg}}) = 104$, this slope would predict that F_C was negative for $T_S < T_S^{\mathrm{avg}} - 17.3 \approx -3°\mathrm{C}$. Since negative values for F_C are unreasonable, and since there likely is still some heat transport even near freezing, instead of a linear function, we have modelled the dependence of F_C on temperature as an hyperbolic function that is nearly zero for temperatures below freezing, and increases roughly linearly for temperatures above freezing. Specifically, we use the function

$$(T_S - T_R) = \frac{1}{2A_1}\left(F_C - \frac{A_2^2}{F_C}\right),$$

or equivalently,

$$F_C(T_S) = A_1(T_S - T_R) + \sqrt{A_1^2(T_S - T_R)^2 + A_2^2}, \tag{A5}$$

where A_1 and A_2 are constants. In terms of the non-dimensional variables and parameters (8), this equation becomes

$$f_C(\tau_S) = a_1(\tau_S - 1) + \sqrt{a_1^2(\tau_S - 1)^2 + a_2^2}. \tag{A6}$$

The constants A_1 and A_2 are chosen so that the forcing at the global average surface temperature T_S^{avg} is 104, and so that the forcing at the freezing point is twenty percent of this value, that is, $F_C(T_R) = 0.2F_C(T_S^{\mathrm{avg}})$. Thus

$$A_2 = 0.2 \cdot 104 = 20.8, \qquad \text{and} \qquad A_1 = \frac{1}{2(T_S^{\mathrm{avg}} - T_R)}\left(104 - \frac{A_2^2}{104}\right) = 3.063, \tag{A7}$$

or in terms of the nondimensional parameters,

$$a_1 = \frac{A_1}{\sigma T_R^3} = 2.650, \qquad \text{and} \qquad a_2 = \frac{A_2}{\sigma T_R^4} = 6.590 \times 10^{-2}. \tag{A8}$$

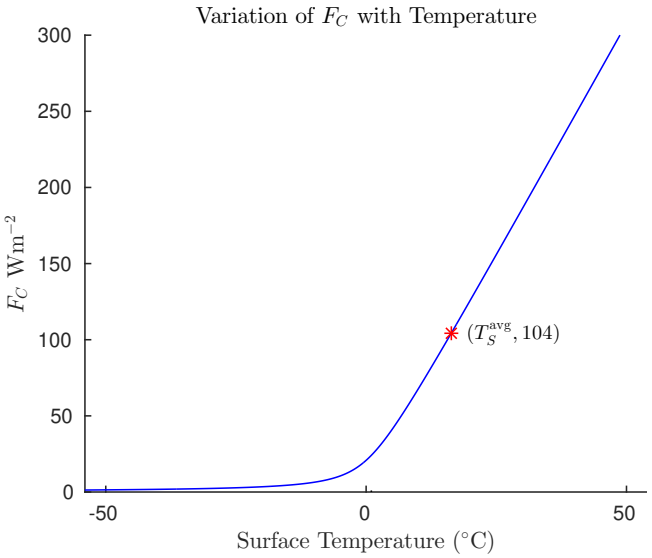

Figure A2. Variation of evapotranspiration/convection with surface temperature. The hyperbolic function is tangent to the horizontal as the temperature decreases, and grows almost linearly with a slope of about 6 as temperature increases.

Figure A2 shows a plot of Equation (A5) for these parameter values. With these choices of the constants, the slope at T_S^{avg} is 5.9, agreeing well the above argument that it should be about 6.

A5 Atmospheric Absorption of Infrared Radiation

Two of the empirical parameters in the EBM are k_W and k_C, defined in Subsection 2.2 as the grey gas absorption coefficients for water vapour and carbon dioxide, respectively. More precisely, the absorption coefficient k of a gas is its proportionality coefficient in the Beer-Lambert Law, as defined in Equation (13) of Subsection 2.2. In the *grey gas approximation*, it is assumed that the absorption coefficient k is constant for all frequencies of incident radiation, and depends only on the total intensity of that radiation. In reality though, k is not an absolute physical constant, because gases absorb radiation at discrete spectral lines. The total amount of energy absorbed depends on the distribution of energy in the radiation at each of these spectral wavelengths. Values of k_W and k_C for the particular spectrum of incident radiation experienced by the atmosphere may be obtained empirically from modern era satellite and land-based measurements. We assume that k_W and k_C for the atmosphere do not change with time, even over the geological timescales considered here.

Atmospheric absorption, η, of infrared radiation emitted by the earth is, in this EBM, attributed to the two primary greenhouse gases: water vapour and carbon dioxide, and to the liquid and solid water making up clouds. According to Trenberth et al. (2009), at present as a global average, the earth emits 398 Wm^{-2} of which 40.1 Wm^{-2} passes through the atmosphere to space. Thus approximately 90 percent of the radiation is absorbed in the atmosphere, that is $\eta = 0.9$. Schmidt et al. (2010) have determined that the present-day absorption factor η can be attributed as follows: Water vapour 50%, Clouds 25% and CO_2 (plus other gases) 25%. Furthermore, they determined that these ratios remain unchanged, even after a doubling of CO_2. Therefore,

setting $x = \eta_C = \eta_{Cl}$ and $\eta_W = 2x$ in Equation (17) we get

$$0.9 = 1 - (1-x)(1-2x)(1-x) = 2x^3 - 5x^2 + 4x.$$

This cubic has one real root, $\hat{x}$,

$$\hat{x} \approx 0.3729. \tag{A9}$$

In this model, since we have no data on cloud cover for paleoclimates, we make the assumption that absorption due to clouds is a constant globally and temporally, and set

$$\eta_{Cl} = \hat{x}. \tag{A10}$$

We also tried varying η_{Cl} with temperature using an hyperbolic function like that used for F_C in (A5), however we found no qualitative change in the results and therefore, for simplicity have left η_{Cl} as a constant. To calibrate the absorption coefficient k_C for the greenhouse gas carbon dioxide, we set $\eta_C = \hat{x}$ in Equation (21) yielding

$$\hat{x} = 1 - e^{-\mu \cdot 1.52\times 10^{-6} k_C P_A/g} \qquad \Longrightarrow \qquad k_C = \frac{g \ln(1-\hat{x})}{\mu(1.52\times 10^{-6})P_A}.$$

Using the present day value of $\mu = 400$ ppm, the value of $\hat{x}$ from (A9), the standard atmospheric pressure value of $P_A = 101.3 \times 10^3$ Pa, and the acceleration due to gravity $g = 9.8$ m s^{-2} we get

$$k_C = \frac{(9.8)\ln(1-\hat{x})}{(400)(1.52\times 10^{-6})(101.3\times 10^3)} = 0.07424 \text{ m}^2 \text{ kg}^{-1}. \tag{A11}$$

With this value for k_C, the coefficient G_C, defined in (20) has the value

$$G_C = 1.52\times 10^{-6} k_C \frac{P_A}{g} = 1.166 \times 10^{-3}. \tag{A12}$$

To calibrate k_W we proceed as follows. The latent heat of vaporization of water is $L_v = 2.2558 \times 10^6$ m^2 s^{-2} and the ideal gas constant specific to water vapour is $R_W = 461.5$ m^2 s^{-2} K^{-1}. Thus from (33) we have

$$G_{W1} = \frac{L_v}{R_W T_R} = 17.89. \tag{A13}$$

Dai (2006) indicates that an average value for relative humidity, δ, from 1976 to 2004 for the region of the earth between 60°S and 75°N is 0.74. Over the same latitudes, Dai reports that averages over water and over land are 0.79 and 0.65, respectively, except that over deserts the humidity drops to 30–50%. The polar regions are typically drier, however, there is a significant amount of water north of 75°N and south of 60°S, hence we have chosen $\delta^{\text{avg}} = 0.74$ as the average global relative humidity for purposes of calibrating k_W. In Equation (34) we set $\eta_W = 2\hat{x}$ with $\hat{x}$ given by (A9), τ_S to the present normalized global average temperature T_S^{avg}/T_R, δ to the present average global relative humidity δ^{avg}, Z to an average global tropopause height

of $Z^{\text{avg}} = 14000$ m, and the normalized lapse rate to $\gamma = \Gamma / T_R = 2.38 \times 10^{-5}\ m^{-1}$. Using these values and inverting (34) to isolate k_W we get

$$k_W = -\ln(1-2\hat{x})\gamma \left[\delta \frac{P_W^{\text{sat}}(T_R)}{R_W T_R} \int_{T_S^{\text{avg}} - \gamma Z^{\text{avg}}}^{T_S^{\text{avg}}} \frac{1}{\tau} \exp\left(G_{W1} \left[\frac{\tau - 1}{\tau} \right] \right) d\tau \right]^{-1} = 0.05905 \text{ m}^2 \text{ kg}^{-1}. \tag{A14}$$

With this value for k_W, the second greenhouse gas parameter for water vapour is

$$G_{W2} \equiv \frac{k_W P_W^{sat}(T_R)}{\gamma R_W T_R} = 12.05. \tag{A15}$$

A6 Atmospheric Emission of Radiation

In previous slab models, including Dortmans et al. (2017) and Payne et al. (2015), it was assumed that the upward and downward radiation intensities from the atmosphere are equal, that is, $\beta = \frac{1}{2}$ in Equation 2. This would be the case for an actual uniform slab; however, the real atmosphere is not uniform in temperature nor density, and in fact both the temperature and density of the atmosphere are much higher in value near the surface than near the tropopause. The net effect of this non-uniformity is that, of the total radiation intensity I_A emitted by the atmosphere, almost two-thirds goes back the surface and only a little more than one-third escapes to space, according to satellite and surface data; see Trenberth et al. (2009); Wild et al. (2013). From Trenberth et al. (2009), the atmosphere and clouds emit $169.9 + 29.9$ Wm^{-2} upward to space and emit 340.3 Wm^{-2} downward to the earth. Therefore, in order to have the model in this paper represent the atmosphere more realistically, we set

$$\beta = \frac{340.3}{340.3 + 169.9 + 29.9} \approx 0.63. \tag{A16}$$

instead of 0.50.

Appendix B: Equilibrium Climate Sensitivity

Equilibrium climate sensitivity (ECS) is a useful measure of the sensitivity of a given climate model to an increase in CO_2 concentration μ. It is usually defined as the change ΔT in the global mean temperature $\bar{T}$, resulting from a doubling of μ, starting from the accepted pre-industrial value $\mu = 270$ ppm; see IPCC (2013); Forster (2016); Knutti et al. (2017); Proistosescu and Huybe . The ECS provides a first-order estimate of the amount of present-day global warming predicted by a given model, as μ increases. Because ECS is a single number, it facilitates comparisons between models. It has been used extensively in the Assessment Reports of the IPCC [IPCC (2013)], where ΔT values in the range 1.5 to 4.5 C have been documented. Some have cited this wide range of ECS values as a sign of weakness of the IPCC methodology. Recently, Proistosescu and Huybers (2017) have reconciled these results. They show that a linear statistical analysis of historical data gives low estimates in the 1.5 to 3 C range, while nonlinear models give higher estimates.

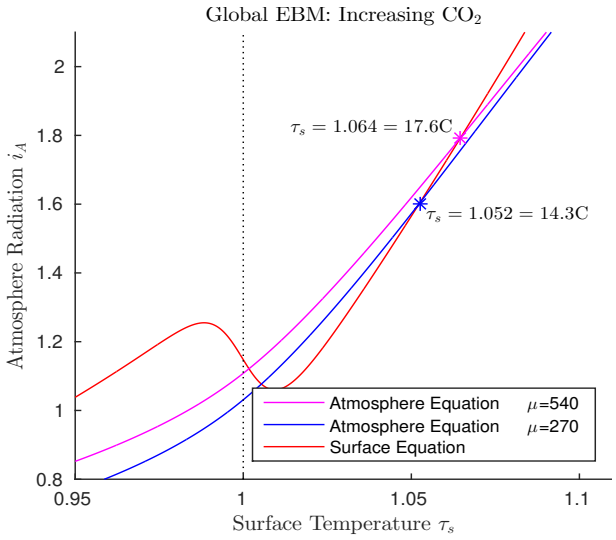

Figure B1. Equilibrium Climate Sensitivity (ECS) for Millennial data. The equilibrium points marked with stars show the change in T_S for a doubling of μ, from 270 to 540 ppm; $T_S(270) = 14.3^\circ$C, $T_S(540) = 17.6^\circ$C, $\Delta T = 3.3^\circ$C.

In terms of our EBM, to apply it to a global average we make the following settings. The global mean insolation at the top of the atmosphere is $Q = 340\,\mathrm{W m^{-2}}$, see Wild et al. (2013); Trenberth et al. (2009). Wild et al. (2013) indicates that $161\,\mathrm{W\ m^{-2}}$ of sunlight is absorbed by the earth while $24\ \mathrm{W\ m^{-2}}$ is reflected back on average. Thus we take

$$\alpha_W = \frac{24}{161+24} = 0.13.$$

For the tropopause height Z we take an average value of $Z^{\mathrm{avg}} = 14$ km. For the global model, the ocean and atmospheric transport terms, F_O and F_A, will be zero.

The ECS value we calculate will be the difference between the warm equilibrium temperatures when $\mu = 270$ and $\mu = 540$. For these calculations we took the relative humidity to be $\delta = \delta^{\mathrm{avg}} = 0.74$, in accord with the value obtained by Dai (2006). The graphs of the surface and atmosphere equilibrium equations are shown in Figure B1. The equilibrium solutions of this global mean version of the EBM yield $T_S(270) = 14.3^\circ$C, $T_S(540) = 17.6^\circ$C, and $\Delta T = 3.3^\circ$C. This is in excellent agreement with accepted values, IPCC (2013).

Code availability. The original Matlab code for the computations that support this research is available in the Appendix of: Dortmans (2017).

Author contributions. W.F. Langford contributed the original hypothesis on which the investigation is based, guided the work, and wrote most of this final paper. B. Dortmans carried out the computations required for this research and wrote an M.Sc. thesis on his work, which

was the starting point for this paper. A.R. Willms co-supervised B. Dortmans' work, significantly extended his calculations, and contributed many insights and guidance for this paper.

Competing interests. The authors declare that they have no conflict of interest.

Acknowledgements. The authors acknowledge financial support of this work by the Natural Sciences and Engineering Research Council of Canada, and thank two anonymous referees for many valuable suggestions. W.F. Langford gratefully acknowledges very helpful discussions with J.F. Basinger and D.R. Greenwood in the early stages of this work.

References

Arnold, L., Namachchivaya, N. Sri and Schenk, K. Toward an understanding of stochastic bifurcation: Case study. Internat. J. Bifur. Chaos 6, (1996) 1947–1979.

Baatsen, M.L.J., von der Heydt, A.S., Huber, M., Kliphuis, M.A., Bijl, P.K., Sluijs, A. and Dijkstra, H. A. Equilibrium state and sensitivity of the simulated middle-to-late Eocene climate. Clim. Past Discuss. doi.org/10.5194/cp-2018-43 (2018)

Ballantyne, A.P., Greenwood, D.R., Sinninghe Damsté, J.S., Csank, A.Z., Eberle, J.J., and Rybczynski, N. Significantly warmer Arctic surface temperatures during the Pliocene indicated by multiple independent proxies. Geology 38, (2010) 603–606.

Barron, E.J., Thompson, S.L. and Schneider, S.H. An ice-free Cretaceous? Results from climate model simulations. Science 212, (1981) 10–13.

Barron, E.J. A warm, equable Cretaceous: the nature of the problem. Earth-Sci. Rev., 19, (1983) 305–338.

Barron, E.J., Fawcett, P.J., Peterson, W.H., Pollard, D. and Thompson, S.L. A "simulation" of mid-Cretaceous climate. Paleoceanography 10, (1995) 953–962.

Bartoli, G., Sarnthein, M., Weinelt, M., Erlenkeuser, H., Garbe-Schönberg, D. and Lea, D.W. Final closure of Panama and the onset of northern hemisphere glaciation. Earth Plan. Sci. Lett. 237, (2005) 33–44.

Bartoli, G., Hönisch, B. and Zeebe R. E. Atmospheric CO_2 decline during the Pliocene intensification of Northern Hemisphere glaciations. Paleoceanography, 26, (2011) PA4213, doi:10.1029/2010PA00205.

Basinger, J.F., Greenwood, D.R. and Sweda, T. Early Tertiary vegetation of Arctic Canada and its relevance to Paleoclimatic interpretation. In: M.C. Boulter and H.C. Fisher, Cenozoic Plants and Climate of the Arctic. NATO ASI Series, Vol. 127, (1994) 175–198, Springer-Verlag.

Bice, K.L., Birgel, D., Meyers, P.A., Dahl, K.A., Hinrichs, K-U., and Norris, R.D. A multiple proxy and model study of Cretaceous upper ocean temperatures and atmospheric CO_2 concentrations. Paleoceanography, 21, (2006). doi:10.1029/2005PA001203

Bowman, V.C., Francis, J.E., Askin, R.A., Riding, J.B. and Swindles, G.T. Latest Cretaceous – earliest Paleogene vegetation and climate change at the high southern latitudes: palynological evidence from Seymour Island, Antarctic Peninsula. Pal. Pal. Pal. 408 (2014) 26–47.

Brierley, C., Burls, N., Ravelo, C. and Fedorov, A. Pliocene warmth and gradients. Nature Geosci. 8 (2015) 419–420.

Briggs, J.C. Biogeography and Plate Tectonics. Elsevier, Amsterdam (1987).

Budyko, M.I. The effect of solar radiation variations on the climate of the Earth. Tellus XXI 5, 611–619 (1968).

Chandan, D. and Peltier, W. R. Regional and global climate for the mid-Pliocene using the University of Toronto version of CCSM4 and PlioMIP2 boundary conditions. Clim. Past 13, (2017) 919–942.

Chandan, D. and Peltier, W. R. On the mechanisms of warming the mid-Pliocene and the inference of a hierarchy of climate sensitivities with relevance to the understanding of climate futures. Clim. Past 14 (2018) 825–856.

Craggs, H.J., Valdes, P.J. and Widdowson, M. Climate model predictions for the latest Cretaceous: An evaluation using climatically sensitive sediments as proxy indicators. Pal. Pal. Pal. 315 (2012) 12–23.

Cronin, T.M. Paleoclimates: Understanding Climate Change Past and Present. Columbia University Press, New York (2010).

Crowley, T. J. Carbon dioxide and Phanerozoic climate. In: Hubert, B. T., MacLead, K. G. and Wing, S. L., Warm Climates in Earth History, Cambridge Univ. Press, Cambridge, UK (2000) 425–444.

Csank, A.z., Patterson, W.P., Eglington, B.M., Rybczynski, N., Basinger, J.F. Climate variability in the Early Pliocene Arctic: annually resolved evidence from stable isotope values of sub-fossil wood, Ellesmere Island, Canada. Pal. Pal. Pal. 398, (2011) 339–349.

Dai, A. Recent Climatology, Variability, and Trends in Global Surface Humidity. Journal of Climate 19, (2006) 3589–3606. DOI: 10.1175/JCLI3816.1

DeConto, R.M., Pollard, D., Wilson, P.A., Pälike, H., Lear, C.H. and Pagani, M. Thresholds for Cenozoic bipolar glaciation. Nature 455, (2008) 652–657.

De Schepper, S., Groeneveld, J., Naafs, B. D. A., Van Renterghem, C., Hennissen, J., Head, M. J., Louwye, S. and Fabian, K. Northern hemisphere glaciation during the globally warm early late Pliocene. PLoS ONE 8 (2013) e81508.

De Schepper, S., Schreck, M., Beck, K.M., Matthiessen, J., Fahl, K. and Mangerud, G. Early Pliocene onset of modern Nordic Seas circulation related to ocean gateway changes. Nature Comm. (2015) 1–8. DOI: 10.1038/ncomms9659

Donnnadieu, Y., Pierrehumbert, R., Jacob, R. and Fluteau, F. Modelling the primary control of paleogeography on Cretaceous climate. EPSL 248 (2006) 426–437.

Dortmans, B. A Conceptual Model of Climate Change Incorporating the Roles of Carbon Dioxide and Water Vapour as Greenhouse Gases. M.Sc. Thesis, Department of Mathematics and Statistics, University of Guelph (2017)

Dortmans, B., Langford, W.F. and Willms, A.R. A conceptual model for the Pliocene paradox. Department of Mathematics and Statistics, University of Guelph, Submitted for publication (2017).

Dowsett, H.J., Haywood, A.M., Valdes, P.J., Robinson, M.M., Lunt, D.J., Hill, D.J., Stoll, D.K. and Foleya, K.M. Sea surface temperatures of the mid-Piacenzian Warm Period: A comparison of PRISM3 and HadCM3. Pal. Pal. Pal. 309 (2011) 83–91.

Dowsett, H.J., Robinson, M.M., Stoll, D.K., Foley, K.M., Johnson, A.L.A., Williams, M. and Riesselman, C.R. The PRISM (Pliocene palaeoclimate) reconstruction: time for a paradigm shift. Phil Trans R Soc A 371 (2013) 20120524.

Dowsett, H., Dolan, A., Rowley, D., Moucha, R., Forte, A.M., Mitrovica, J.X., Pound, M., Salzmann, U., Robinson, M., Chandler, M. Foley, K. and Haywood, A. The PRISM4 (mid-Piacenzian) paleoenvironmental reconstruction. Clim. Past 12 (2016) 1519–1538.

Fedorov, A. V., Dekens, P. S., McCarthy, M., Ravelo, A. C., deMenocal, P. B., Barreiro, M., Pacanowski, R. C. and Philander, S. G. The Pliocene paradox (Mechanisms for a permanent El Niño). Science 312, (2006) 1485–1489.

Fedorov, A.V., Brierley, C.M. and Emanuel, K. Tropical cyclones and permanent El Niño in the early Pliocene epoch. Nature 463, (2010) 1066–1070.

Ferreira, D., Marshall, J., and Rose, B. Climate determinism revisited: Multiple equilibria in a complex climate model. J. Climate 24, (2011) 992–1012.

Fletcher, B.J., Brentnall, S. J., Anderson, C. W., Berner, R. A. and Beerling, D. J. Atmospheric carbon dioxide linked with Mesozoic and early Cenozoic climate change. Nature Geoscience 1, (2008) 43–48.

Fletcher, T., Warden, L., Damsté, J.S.S., Brown, K.J., Rybczynski, N., Gosse, J. and Ballantyne, A. P. The role of elevated atmospheric CO_2 and increased fire in Arctic amplification of temperature during the Early to mid-Pliocene. Clim. Past Discuss. 2018–60. doi.org/10.5194/cp-2018-60

Forster, P. Inference of Climate Sensitivity from Analysis of Earth's Energy Budget. Ann. Rev. Earth Planet. Sci. 44, (2016) 85–106.

Fretwell, P., Pritchard, H. D., Vaughan, D. G., Bamber J. L., Barrand, N. E., Bell, R., Bianchi, C., Bingham, R. G., Blankenship, D. D., Casassa, G., Catania, G., Callens, D., Conway, H., Cook, A. J., Corr, H. F. J., Damaske, D., Damm, V., Ferraccioli, F., Forsberg, R., Fujita, S., Gim, Y., Gogineni, P., Griggs, J. A., Hindmarsh,R. C. A., Holmlund, P. J., Holt, W., Jacobel, R. W., Jenkins, A., Jokat, W., Jordan, T., King, E. C., Kohler, J., Krabill, W., Riger-Kusk, M., Langley, K. A., Leitchenkov, G., Leuschen, C., Luyendyk, B. P., Matsuoka, K., Mouginot, J., Nitsche, F. O., Nogi, Y., Nost, O. A., Popov, S. V., Rignot2, E., Rippin, D. M., Rivera, A., Roberts, J., Ross, N., Siegert, M.

J., Smith, A. M., Steinhage, D., Studinger, M., Sun, B.,Tinto, B. K., Welch, B. C., Wilson, D., Young, D. A., Xiangbin, C., and Zirizzotti, A. Bedmap2: improved ice bed, surface and thickness datasets for Antarctica. Cryosphere 7, (2013) 375–393.

Goldner, A., Herold, N. and Huber, M. Antarctic glaciation caused ocean circulation changes at the ~~Eocene?Oligocene~~ Eocene–Oligocene transition. Nature 511, (2014) 574–577.

Greenwood, D. R., Basinger, J. F. and Smith, R. Y. How wet was the Arctic Eocene rain forest? Estimates of precipitation from Paleogene Arctic macrofloras. Geology 38, (2010) 15–18.

Haug, G.H., Tiedemann, R. and Keigwin, L.D. How the Isthmus of Panama put ice in the Arctic. Oceanus 42, (2004) 1–4.

Haywood, A.M., Dowsett, H.J., Valdes, P.J., Lunt, D.J., Francis, J.E. and Sellwood, B.W. Introduction. Pliocene climate, processes and problems. Phil Trans. R. Soc. A 367 (2009) 3–17.

Haywood, A. M., Dowsett, H. J., Robinson, M. M., Stoll, D. K., Dolan, A. M., Lunt, D. J., Otto-Bliesner, B. and Chandler, M. A. Pliocene Model Intercomparison Project (PlioMIP): experimental design and boundary conditions (Experiment 2) Geosci. Model Dev. 4, (2011) 571–577.

Haywood, A.M., Dowsett, H.J., Dolan, A.M., Rowley, D., Abe-Ouchi, A., Otto-Bliesner, B., Chandler, M.A., Hunter, S.J., Lunt, D.J., Pound, M. and Salzmann, U. The Pliocene Model Intercomparison Project (PlioMIP) Phase 2: scientific objectives and experimental design. Clim. Past, 12, (2016) 663–675.

Heydt, A.S. von der and Dijkstra, H.A. El Niño in the Pliocene. NatureGeosci. 4 (2011) 502–503.

Huber, M. and Caballero R. The early Eocene equable climate problem revisited. Clim. Past 7, (2011) 603–633.

Hubert, B. T., MacLead, K. G. and Wing, S. L., Warm Climates in Earth History, Cambridge Univ. Press, Cambridge, UK (2000).

Hutchinson, D.K., de Boer, A.M., Coxall, H.K., Caballero, R., Nilsson, J. and Baatsen, M. .Climate sensitivity and meridional overturning circulation in the late Eocene using GFDL CM2.1 Clim. Past, 14, (2018) 789–810.

Intergovernmental Panel on Climate Change. Climate Change 2013: The Physical Science Basis. Contribution of Working Group I to the Fifth Assessment Report of the Intergovernmental Panel on Climate Change. [Stocker, T.F., D. Qin, G.-K. Plattner, M. Tignor, S.K. Allen, J. Boschung, A. Nauels, Y. Xia, V. Bex and P.M. Midgley (eds.)]. Cambridge University Press, Cambridge, United Kingdom and New York, NY, USA, (2013) 1535 pp. [Also available at http://www.ipcc.ch/]

International Civil Aviation Organization. Manual of the ICAO Standard Atmosphere: extended to 80 kilometres. Third Edition. ICAO, 1000 Sherbrooke Street West Suite 400, Montreal, Quebec, Canada H3A 2R2 (1993)

Jahren, A.H., and Sternberg, L.S.L., Humidity estimate for the middle Eocene Arctic rain forest. Geology 31, (2003) 463–466.

Kaper, H. and Engler, H. Mathematics and Climate. Society for Industrial and Applied Mathematics, Philadelphia USA (2013)

Katz, M.E., Miller, K.G., Wright, J.D., Wade, B.S., Browning, J.V., Cramer, B.S. and Rosenthal, Y. Stepwise transition from the Eocene greenhouse to the Oligocene icehouse. Nature Geoscience Vol. 1, (2008) 329–334.

Kishore, P., Namboothiri, S.P., Igarashi, K., Jiang, Jonathan H., Ao, Chi O., and Romans, Larry J. Climatological characteristics of the tropopause parameters derived from GPS/CHAMP and GPS/SAC-C measurements. J. Geophys. Res., 111, (2006) doi:10.1029/2005JD006827

Knies, J., Cabedo-Sanz, P., Belt, S.T., Baranwal, S., Fietz, S. and Rosell-Melé, A. The emergence of modern sea ice cover in the Arctic Ocean. Nature Comm. (2014) DOI: 10.1038/ncomms6608

Knutti, R., Rugenstein, M.A.A. and Hegerl, G.C. Beyond equilibrium climate sensitivity. Nature Geo. 10 (2017) 727–736.

Kuznetsov, Y.A. Elements of Applied Bifurcation Theory. Third Edition. Springer, New York, (2004).

Ladant, J.-B. and Donnadieu, Y. Palaeogeographic regulation of glacial events during the Cretaceous supergreenhouse. Nature Comm. DOI: 10.1038/ncomms12771 (2016)

Ladant, J.-B., Donnadieu, Y., Lefebvre, V. and Dumas, C. The respective role of atmospheric carbon dioxide and orbital parameters on ice sheet evolution at the Eocene-Oligocene transition. Paleoceanography 29 (2014) 810–823.

Langford, W.F. and Lewis, G.M. Poleward expansion of Hadley cells. Can. Appl. Math. Quart. 17, (2009) 105–119.

Lawrence, K. T., Herbert, T. D., Brown, C. M., Raymo, M. E. and Haywood, A. M. High-amplitude variations in North Atlantic sea surface temperature during the early Pliocene warm period, Paleoceanography, 24, (2009) PA2218.

Lear, C.H., Bailey, T.R., Pearson, P.N., Coxall, H.K. and Rosenthal, Y. Cooling and ice growth across the Eocene-Oligocene transition. Geology 36 (2008) 251–254.

Lewis, G.M. and Langford, W.F. Hysteresis in a rotating differentially heated spherical shell of Boussinesq fluid. SIAM J. Appl. Dyn. Syst. 7, (2008) 1421–1444.

Lunt, D.J., Farnsworth, A., Loptson, C., Foster, G.L., Markwick, P., O'Brien, C.L., Pancost, R.D., Robinson, S.A. and Wrobel, N. Palaeogeographic controls on climate and proxy interpretation. Clim. Past, 12, (2016) 1181–1198.

Lunt, D.J., Foster, G.L., Haywood, A.M. and Stone, E.J. Late Pliocene Greenland glaciation controlled by a decline in atmospheric CO_2 levels. Nature 454 (2008) 1102–1105.

Lunt, D.J., Huber, M., Anagnostou, E., Baatsen, M.L.J., Caballero, R., DeConto, R., Dijkstra, H.A., Donnadieu, Y., Evans, D., Feng, R., Foster, G.L., Gasson, E., von der Heydt, A.S., Hollis, C.J., Inglis, G.N., Jones, S.M., Kiehl, J., Turner, S.K., Korty, R.L., Kozdon, R., Krishnan, S., Ladant, J.-B., Langebroek, P., Lear, C.H., LeGrande, A.N., Littler, K., Markwick, P., Otto-Bliesner, B., Pearson, P., Poulsen, C.J., Salzmann, U., Shields, C., Snell, K., Stärz, M., Super, J., Tabor, C., Tierney, J.E., Tourte, G.J.L., Tripati, A., Upchurch, G.R., Wade, B.S., Wing, S.L., Winguth, A.M.E., Wright, N.M., Zachos, J.C. and Zeebe, R.E. The DeepMIP contribution to PMIP4: experimental design for model simulations of the EECO, PETM, and pre-PETM (version 1.0). Geosci. Model Dev., 10, (2017) 889–901.

Martínez-Botí, M.A., Foster, G. L., Chalk, T. B., Rohling, E. J., Sexton, P. F., Lunt, D. J., Pancost, R. D., Badger, M. P. S., and Schmidt, D. N. Plio-Pleistocene climate sensitivity evaluated using high-resolution CO2 records. Nature 518 (2015) 49–54.

McGehee, R. and Lehman, C. A paleoclimate model of ice-albedo feedback forced by variations in Earth's orbit. SIAM J. Appl. Dynam. Sys. 11, (2012) 684–707.

Miller, K. G., Browning, J. V., Aubry, M-P., Wade, B. S., Katz, M. E., Kulpecz, A. A. and Wright, J. D. Eocene–Oligocene global climate and sea-level changes: St. Stephens Quarry, Alabama. GSA Bulletin 120 (2008) 34–53.

Namachchivaya, N. Sri. Stochastic Bifurcations. J. Appl. Math. Comput., 38, (1990) 101–159.

North, G.R., Cahalan, R.F. and Coakley, J.A. Energy balance climate models. Rev. Geophys. Space Phys. 19, (1981) 91–121.

O'Brien, C.L., Foster, G.L., Martinez-Botí, M.A., Abell, R., Rae, J.W.B. and Pancost, R.D. High sea surface temperatures in tropical warm pools during the Pliocene. Nature Geosci. 7 (2014) 606–611.

O'Brien, C. L., Robinson, S. A., Pancost, R. D., Damsté, J. S. S., Schouten, S., Lunt, D. J., Alsenz, H., Bornemann, A., Bottini, C., Brassell, S. C., Farnsworth, A., Forster, A., Huber, B. T., Inglis, G. N., Jenkyns, H. C., Linnert, C., Littler, K., Markwick, P., McAnena, A., Mutterlose, J., Naafs, B. D. A., Püttmann, W., Sluijs, A., van Helmond, N. A. G. M., Vellekoop, J., Wagner, T. and Wrobel, N. E. Cretaceous sea-surface temperature evolution: Constraints from TEX_{86} and planktonic foraminiferal oxygen isotopes. Earth Sci. Rev. 172, (2017) 224–247.

Pagani, M., Arthur, M. A. and Freeman, K. H. Miocene evolution of atmospheric carbon dioxide. Paleoceanography 14, (1999) 273–292.

Pagani, M., Caldeira, K., Archer, D. and Zachos, K. C.. An ancient carbon mystery. Science 314, (2006) 1556–1557.

Pagani, M., Huber, M., Liu, Z., Bohaty, S.M., Henderiks, J., Sijp, W., Krishnan, S. and DeConto, R.N. The role of carbon dioxide during the onset of Antarctic glaciation. Science 334, (2011) 1261–1264.

Pagani, M., Zachos, J.C., Freeman, K.H., Tipple, B. and Bohaty, S. Marked decline in atmospheric carbon dioxide concentrations during the Paleogene. Science 309, (2005) 600–603.

Paillard, D. The timing of Pleistocene glaciations from a simple multiple-state climate model. Nature 391, (1998) 378–381.

Payne, A. E., Jansen, M. F. and Cronin, T. W. Conceptual model analysis of the influence of temperature feedbacks on polar amplification. Geophys. Res. Lett. 42, (2015) 9561–9570.

Pierrehumbert, R.T. Principles of Planetary Climate. Cambridge University Press, Cambridge UK (2010)

Proistosescu, C. and Huybers P.J. Slow climate mode reconciles historical and model-based estimates of climate sensitivity. Sci. Adv. 3, (2017) e1602821.

Ruddiman, W.F. Earth's Climate Past and Future. Third Edition. W.H. Freeman and Company (2014)

Sagan, C. and Mullen, G. Earth and Mars: Evolution of atmospheres and surface temperatures. Science, New Series, 177, (1972) 52–56.

Salzmann, U., Haywood, A.M. and Lunt, D.J. The past is a guide to the future? Comparing Middle Pliocene vegetation with predicted biome distributions for the twenty-first century. Phil Trans. R. Soc. A 367 (2009) 189–204.

Scher, H. D., Bohaty, S. M., Zachos, J. C. and Delany, M. L. Two-stepping into the icehouse: East Antarctic weathering during progressive ice-sheet expansion at the Eocene–Oligocene transition. Geology 39, (2011) 383–386.

Scher, H.D., Whittaker, J.M., Williams, S.E., Latimer, J.C., Kordesch, W.E.C. and Delaney, M.L. Onset of Antarctic Circumpolar Current 30 million years ago as Tasmanian Gateway aligned with westerlies. Nature 523, (2015) 580–583.

Schmidt, G.A., Ruedy, R.A., Miller, R.L. and Lacis, A.A. Attribution of the present-day total greenhouse effect. J. Geophys. Res. 115, (2010) doi:10.1029/2010JD014287.

Seki, O., Gavin L. Foster, G.L., Schmidt, D.N., Mackensen, A., Kawamura, K. and Pancost, R.D. Alkenone and boron-based Pliocene pCO_2 records. Earth and Planetary Science Letters 292 (2010) 201–211.

Sellers, W. D. A global climate model based on the energy balance of the earth-atmosphere system. J. Appl. Meteo. 8, (1969) 392–400.

Sloan, S. B. and Barron, E. J. "Equable" climates during Earth history? Geology 18, (1990) 489–492.

Sloan, S. B. and Barron, E. J. A comparison of Eocene climate model results to quantified paleoclimatic interpretations. Pal. Pal. Pal. 93, (1992) 183–202.

Sloan, S. B. and Rea, D. K. Atmospheric carbon dioxide and early Eocene climate: A general circulation modeling sensitivity study. Pal. Pal. Pal. 119, (1995) 275–292.

Stap, L.B., van de Wal, R.S.W., de Boer, B., Bintanja, R. and Lourens, L.J. The influence of ice-sheets on temperature during the past 38 million years inferred from a one-dimensional ice sheet-climate model. Clim. Past 13, (2017) 1243–1257.

Steph, S., Tiedemann, R., Prange, R.M., Groeneveld, J., Schulz, M., Timmermann, A., Nürnberg, D., Rühlemann, C., Saukel, C. and Haug, G.H. Early Pliocene increase in thermohaline overturning: A precondition for the development of the modern equatorial Pacific cold tongue. Paleoceanography 25 (2010) PA2202, doi:10.1029/2008PA001645

Struzik, E. Future Arctic: Field Notes from a World on the Edge. Island Press, Washington, DC (2015)

Sun, Y., Ramstein, G., Contoux, C. and Zhou, T. A comparative study of large-scale atmospheric circulation in the context of a future scenario (RCP4.5) and past warmth (mid-Pliocene). Clim. Past 9, (2013) 1613–1627.

Tan, N., Ramstein, G., Dumas, C., Contoux, C., Ladant, J.-B., Sepulchre, P., Zhang, Z., and De Schepper, S. Exploring the MIS M2 glaciation occurring during a warm and high atmospheric CO_2 Pliocene background climate. EPSL 472, (2017) 266–276.

Tedford, R.H. and Harington, C.R. An Arctic mammal fauna from the Early Pliocene of North America. Nature 425, (2003) 388–390.

Thorndike, A. Multiple equilibria in a minimal climate model. Cold Reg. Sci. Technol. 76, (2012) 3–7. doi:10.1016/j.coldregions.2011.03.002

Trenberth, K.E., Fasullo, J.T. and Kiehl, J. Earth's global energy budget. Bull. AMS 90, (2009) 311–323.

Wang, K., Dickinson, R. E., Wild, M. and Liang, S. Evidence for decadal variation in global terrestrial evapotranspiration between 1982 and 2002: 2. Results. J. Geophys. Res. 115, (2010) D20113

Watanabe, T., Suzuki, A., Minobe, S., Kawashima, T., Kameo, K., Minoshima, K., Aguilar, Y.M., Wani, R., Kawahata, H., Sowa, K., Nagai, T. and Kase T. Permanent El Niño during the Pliocene warm period not supported by coral evidence. Nature 471, (2011) 209–211.

West, C.K., Greenwood, D.R. and Basinger, J.F. Was the Arctic Eocene 'rainforest' monsoonal? Estimates of seasonal precipitation from early Eocene megafloras from Ellesmere Island, Nunavut. EPSL 427, (2015) 18–30.

Wild, M., Folini, D., Schär C., Loeb, N., Dutton, E.G. and König-Langlo, G. The global energy balance from a surface perspective. Clim. Dyn. 40, (2013) 3107–3134.

Willeit, M., Ganopolski, A., Calov, R., Robinson, A. and Maslin, M. The role of CO_2 decline for the onset of Northern Hemisphere glaciation. Quaternary Sci. Rev. 119 (2015) 22–34.

Wing, S.L. and Greenwood, D.R. Fossils and fossil climate: the case for equable climate interiors in the Eocene. Phil. Trans. Roy. Soc. B 341, (1993) 243–252.

Wolfe, A. E., Reyes, A.V., Royer, D. L., Greenwood, D. R., Doria, G., Gagen, M. H., Siver, P. A., and Westgate, J. A. Middle Eocene CO2 and climate reconstructed from the sediment fill of a subarctic kimberlite maar. Geology 45, (2017) 619–622.

Zhang, Z.-S. and Yan, Q. Pre-industrial and mid-Pliocene simulations with NorESM-L: AGCM simulations. Geosci. Model Dev. 5, (2012) 1033–1043.

Zhang, Z.-S., Nisancioglu, K.H., Chandler, M. A., Haywood, A. M., Otto–Bliesner, B. L., Ramstein, G., Stepanek, C., Abe-Ouchi, A., Chan, W.-L., Bragg, F. J., Contoux, C., Dolan, A. M., Hill, D. J., Jost, A., Kamae, Y., Lohmann, G., Lunt, D. J., Rosenbloom, N. A., Sohl, L. E. and Ueda, H. Mid-Pliocene Atlantic Meridional Overturning Circulation not unlike modern. Clim. Past 9, (2013) 1495–1504.